Structure, biochemical characterization and analysis of the pleomorphism of carboxylesterase Cest-2923 from *Lactobacillus plantarum* WCFS1

Rocío Benavente[1], María Esteban-Torres[2], Iván Acebrón[1], Blanca de las Rivas[2], Rosario Muñoz[2], Yanaisis Álvarez[1] and José Miguel Mancheño[1]

1 Department of Crystallography and Structural Biology, Institute of Physical Chemistry Rocasolano, CSIC, Serrano 119, E-28006 Madrid, Spain

2 Laboratory of Bacterial Biotechnology, Institute of Food Science and Technology and Nutrition (ICTAN), CSIC, Juan de la Cierva 3, E-28006 Madrid, Spain

Keywords

α/β hydrolase; analytical ultracentrifugation; esterase; pleomorphism; X-ray crystallography

Correspondence

J.M. Mancheño, Department of Crystallography and Structural Biology, Institute of Physical Chemistry Rocasolano, CSIC, Serrano 119, E-28006 Madrid, Spain

Tel: +34-917459547

Fax: +34-5642431

E-mail: xjosemi@iqfr.csic.es

Running title

Structure and associative behaviour of Cest-2923.

Database

The atomic coordinates and structure factors have been deposited in the Protein Data Bank with accession numbers: **4BZW** for Cest-2923 from native crystals not soaked with substrates ($P6_322$ space group); **4C01** for Cest-2923 from crystals soaked with phenyl acetate ($C2$ space group); **4BZZ** for Cest-2923 from crystals soaked with isopropenyl acetate ($P622$ space group)

Abstract

The α/β hydrolase fold is one of the most versatile structures in the protein realm according to the diversity of sequences adopting such a three dimensional architecture. Here, we report the crystal structure of the carboxylesterase Cest-2923 from the lactic acid bacterium *Lactobacillus plantarum* WCFS1 refined to 2.1 Å resolution, determined its main biochemical characteristics and also carried out an analysis of its associative behaviour in solution. We found that the versatility of a canonical α/β-hydrolase fold, the basic framework of the crystal structure of Cest-2923, also extends to its oligomeric behavior in solution. Thus, we discovered that Cest-2923 exhibits a pH-dependent pleomorphic behaviour in solution involving monomers, canonical dimers and tetramers. Whereas at neutral pH the system is mainly shifted to dimeric species, at acidic conditions tetrameric species predominate. Interestingly, despite that these tetramers result from the association of canonical dimers, as commonly found in many other carboxylesterases from the hormone-sensitive lipase family, they can be defined as "non canonical" since they represent a different association mode. We identified this same type of tetramers in the closest relative of Cest-2923 structurally characterized, the sugar hydrolase YeeB from *Lactococcus lactis*. Interestingly, the observed associative behaviour is consistent with different crystallographic results of Cest-2923 from structural genomics consortia. Finally, we benefit from the presence of sulphate or acetate molecules (depending on the crystal form analysed) in the close vicinity of the nucleophile Ser116, to identify interactions with the putative oxyanion hole and also to deduce the existence of hydrolytic activity within Cest-2923 crystals.

Introduction

Carboxylesterases (EC 3.1.1.1) are enzymes widely distributed in animals, plants and microorganisms [1] that hydrolyse (synthesize) carboxylic esters. Specifically, the term carboxylesterase is adopted for enzymes acting on soluble, monomeric (e.g. below their critical micellar concentration) substrates, in contrast to lipases (EC 3.1.1.3), which display maximal activity against water-insoluble substrates [2, 3]. Based on their amino acid sequences and in particular in the presence of specific sequence motifs esterases and lipases are classified into four blocks, C, H, L and X [4]. Block H includes the plant carboxylesterase and hormone-sensitive lipase (HSL) families. The members of this latter family are distributed over all kingdoms of life and share sequence similarity to mammalian HSL [5]. Family IV of a previous classification of bacterial lipolytic enzymes [3] corresponds to the bacterial members of the HSL family.

Structurally, carboxylesterases belong to the α/β hydrolase superfamily of enzymes [6-8]. The crystal structures currently determined for members of this superfamily (524 PDB entries using the term α/β hydrolase fold from the SCOP classification) reveal a highly conserved protein architecture, the α/β hydrolase fold, a central, mostly parallel β-sheet, surrounded on both sides by α–helices. In all cases, the catalytic machinery is based on a highly conserved catalytic triad made up of a nucleophile (serine), an acid (Asp/Glu) and a histidine. The nucleophile is located in the so-called nucleophile elbow [8], which together with the "oxyanion hole" involved in the stabilization of the negatively charged tetrahedral intermediates, are the hallmarks of the α/β hydrolases.

One remarkable feature of the α/β hydrolase fold is its structural versatility: on the one hand, sequences with very low level of similarity (< 20 %) adopt essentially the same structural core and, on the other, it means that large domains can be added to this fold, which remains as an easily identifiable, conserved core. Usually these new domains are inserted between the canonical strands β6 and β7 and are believed to modulate specific properties of the enzyme [7,8].

Although lactic acid bacteria (LAB) play an important role in the production of fermented food products [9], little information exists about LAB as a source of enzymes [10]. In this regard, the recently reported genome of *Lactobacillus plantarum* WCFS1 [11] reveals the existence of numerous ORFs

coding putative esterases, among them the gene coding for the putative carboxylesterase Cest-2923 (*lp_2923)*. This enzyme has been recently crystallized by two independent structural genomics consortia (Joint Center for Structural Genomics, JCSG, and NorthEast Structural Genomics Consortium, NESG), which reported incomplete models for the enzyme (PDB entries: 3bxp for JCSG and 3d3n for NESG), which as revealed herein show features in conflict with the presence of the canonical catalytic triad.

Here, we report the complete crystal structure of Cest-2923, which as expected from sequence comparisons and the structural data from the above structural genomics consortia, exhibits a canonical α/β hydrolase fold. In addition, our biophysical studies reveal that the enzyme shows complex pH-dependent pleomorphic behaviour in solution. Finally, we have determined the main biochemical features of Cest-2923, which demonstrate that the enzyme is a true carboxylesterase as expected from the genome annotation.

Results and discussion

General comments about search models and description of the monomer structure

N-terminally His-tagged Cest-2923 when overexpressed using the pURI3-TEV vector as in our previous structural studies [12] turned out to be marginally stable in solution and therefore not suitable for crystallization experiments. On the contrary, the C-terminally His-tagged variant behaved well in solution and was suitable for crystallization. The enzyme crystallized in the hexagonal space group $P6_322$ (unit-cell dimensions $a = b = 141.65$ Å, $c = 165.74$ Å, $\alpha = \beta = 90^{\circ}$, $\gamma = 120^{\circ}$) with two independent protein molecules per asymmetric unit. Diffraction data up to 2.1 Å resolution were measured at beamline ID29 at the ESRF (Grenoble, France) on a Pilatus 6M detector, and the structure of the esterase has been solved by molecular replacement. At that moment there were two sets of atomic coordinates for Cest-2923 in the Protein Data Bank, one deposited by the Northeast Structural Genomics Consortium (PDB code: 3d3n) and the other one by the Joint Center for Structural Genomics (PDB code: 3bxp). Previous inspection of these models revealed two aspects: first, the two independent molecules of the corresponding asymmetric units were incomplete, lacking a catalytically relevant region around residues Gly231 to Tyr250, and second and most remarkably, they exhibited structural features incompatible with the presence of the catalytic triad typical of an α/β-hydrolase fold, which is the basic architecture of this enzyme. These latter anomalous features will be treated in detail below. Only the shortest deposited model for Cest-2923 (molecule A from the PDB entry 3d3n) is devoid of these anomalous structural features and therefore used as search model. This model lacks the 25-residue sequence stretch between residues Gly231 and Ala255, in conflict with the classic definition of the catalytic triad since it contains the catalytic residue His233 (see below), plus a 3-residue loop (Phe28-Thr30).

In this regard, the residues forming the catalytic triad of Cest-2923 (Ser116, His233 and Asp201) were predicted in a straightforward manner from a simple BLAST search against the PDB, which in turn revealed the putative sugar hydrolase YeeB from *Lactococcus lactis* (PDB entry 3hxk) and the carboxylesterase lp_1002 (PDB entry 3bjr) as the closest homologs (33 and 32% sequence identity, respectively) structurally characterized (**Fig 1**).

The two Cest-2923 independent molecules making up the asymmetric unit of our hexagonal crystal are essentially identical (0.36 Å rmsd for 275 Cα atoms). We arbitrarily chose chain A as reference for description of the protein. As indicated above, the structure of the Cest-2923 subunit is based on a canonical α/β hydrolase fold [6-8] consisting of a central eight-stranded β-sheet, with strand β2 being the only antiparallel strand (**Fig. 2**). The β-sheet shows a marked left-handed twist with an approximate angle of 90º between strands β1 and β8. This core is surrounded by five helices with α1 (Ala54-Met61) and α7 (Trp258-Glu268) lying in one side of the sheet and α2 (Trp84-His103), α3 (Ala117-Val128) and α6 (Ile207-Gln218) on the opposite one. Although Cest-2923 is currently classified as member of the hormone-sensitive lipase subfamily (HSL) of α/β hydrolases [13] by the ESTHER database, the enzyme does not exhibit a distinct cap domain over the active site. Curiously, the loop between strand β8 (Thr223-Phe228) and helix α7 is highly flexible as deduced from the above mentioned models from the JCSG and NESG consortia for the enzyme where this region cannot be modelled, and may perhaps function as a pseudo-flap.

Comparison with other esterases

A DALI search [14] revealed numerous structures with high structural similarity, as otherwise expected due to the high level of conservation of the α/β hydrolase fold [6-8]. Sugar hydrolase YeeB from *Lactococcus lactis* (PDB entry: 3hxk) and carboxylesterase lp_1002 from *Lactobacillus plantarum* WCFS1 (PDB entry: 3bjr) have the highest structural similarity (*Z*-score = 34.7 and 28.8; rmsd = 1.5 and 2.0 Å for 250 and 244 Cα atoms, respectively). Other esterases from the HSL subfamily such as Est1 from environmental samples [15], Sto-Est from *Sulfolobus tokodaii* [16], PestE from *Pyrobaculum calidifontis* [17] and acetyl esterase from *Salmonella typhimurium* (PDB entry: 3ga7) are also structurally similar (*Z*-score = 25.4, 24.8, 24.6 and 24.5; rmsd = 2.5, 2.6, 2.5 and 2.6 Å for 236, 236, 234 and 240 Cα atoms, respectively). In these latter cases, the structural similarity is limited to the α/β hydrolase fold (core β-sheet plus the two surrounding layers of α-helices), since as above indicated Cest-2923 lacks a cap domain characteristic of some HSL enzymes.

Definition of the active site of Cest-2923: the catalytic triad

As a member of the α/β hydrolase superfamily, the catalytic machinery of Cest-2923 is based on a catalytic triad formed by Ser, His, and Asp/Glu residues (Ser116, His233 and Asp201), which are located at canonical sites along the protein sequence. The nucleophile Ser116 of Cest-2923 is situated in the so-called nucleophilic elbow, within a highly conserved sequence (Gly-X-Ser-X-Gly) (with X denoting any amino acid) [13], with its backbone angles residing in an unfavourable region of the Ramachandran plot ($\phi = 52^{o}$, $\psi = -118^{o}$). This constrained conformation is stabilized by a dense network of hydrogen bonds affecting both to the polypeptide chain (two 2.9 Å hydrogen bonds between the carbonyl oxygen atom and the amide nitrogen atoms of Gly119 and Val156, respectively, and a 3.0 Å hydrogen bond between the amide nitrogen atom of Ser116 and the carbonyl oxygen of Gly153), and to the hydroxyl side chain (a hydrogen bond (2.8 Å) between the Oγ atom and the Nε2 atom of His233) (**Fig 3a**).

The proton carrier residues His233 and Asp201 of the charge-relay system locate downstream the strands β8 and β7, respectively. Particularly, the amino acid His233 is located within the 29-residue long loop connecting strand β8 to helix α7. The Nδ1 atom of His233 is hydrogen bonded to the Oδ1 atom (2.7 Å) and to the Oδ2 atom (3.1 Å) of Asp201. The conformation of this last side chain is further stabilized by a hydrogen bond between the Oδ2 atom and the NH of Val204 (2.9 Å) and is also at hydrogen bond distance to the CO of this latter residue (3.1 Å). In addition, the Oδ1 atom is hydrogen bonded to the Nε2 atom of Gln197 (3.0 Å) and also to a highly ordered water molecule (2.7 Å). This solvent molecule together with its close interacting neighbour (2.9 Å distance between them) are present in all structural homologs of Cest-2923 found with DALI and have been proposed to play a structural role in this family of enzymes [18]. In particular, in Cest-2923 these solvent molecules may contribute to maintain the proper conformation of this part of the active site by bridging the loops where His233 and Asp201 are situated. Thus, molecule HOH45 hydrogen bonds to NH atom (3.0 Å) and to the Oγ1 atom (2.8 Å) of Thr198 from the loop connecting strand β7 to helix α6, and HOH4 makes hydrogen bonds to the NH atom (3.1 Å) of Leu235 and to the CO atom (2.8 Å) of Ile232 from the loop between strand β8 and helix α7.

Interestingly, a spherical blob of electron density appeared in close contact to the hydroxyl group of the nucleophile Ser116 of both independent molecules that has been assigned to a sulphate molecule coming from the crystallization solution (**Fig. 3b**). This molecule may be claimed to mimic the negatively charged tetrahedral intermediates of the catalytic reaction, which are stabilized by the so-called oxyanion hole [7]. In this case, the sulphate molecule is stabilized by polar interactions with amide nitrogen atoms of Gly43, Gly44 and Ala117, what would suggest the existence of a tridentate oxyanion hole similar to those from heroin esterase [19], esterase EstE1 [15] or carboxylesterase EST2 from *Alicyclobacillus acidocaldarius* [18], in contrast to the most commonly observed bidentate counterparts [7].

As above indicated, the atomic models of Cest-2923 deposited by the JCSG and NESG consortia (PDB entries 3d3n and 3bxp, respectively), exhibited structural features which are incompatible with the presence of a catalytic triad (**Fig. S1)**. Specifically, in molecule A from PDB entry 3d3n, which is the shortest model, the Asp201 side chain location overlaps with that of His233 (in our model), which in this model is not defined (**Fig. S1a**). Conversely, the trace of the loop that contains the catalytic residue His233 in molecule B places this residue at a distance of 15 Å from the nucleophile Ser116 (distance between Cα atoms), a geometry incompatible with the built-up of a catalytic triad (**Fig. S1b**). Conversely, the conformation of the connecting loop between strand β7 and helix α6 almost coincides with our model, placing the catalytic Asp201 in a similar position. Similar anomalous structural features can be detected in molecules A and B from PDB entry 3bxp (**Fig. S1b**): in this case, the trace of the connecting loop between strand β7 and helix α6 from molecule A places Asp233 in a wrong position and orientation, preventing the catalytic His233 residue to be located in its proper, canonical position, close to the nucleophile Ser116 (**Fig. S1c**). Finally, similar features can be identified in molecule B (**Fig. S1d**).

Oligomeric states of Cest_Lp2923: a case of pH-dependent pleomorphism

The two molecules in the asymmetric unit of the Cest-2923 hexagonal crystal tightly associate, forming a dimer. The association mode is similar to the one observed for other dimeric esterases from the α/β hydrolase superfamily [16, 17] and involves the antiparallel association between β8 strands and interactions between helices preceding (α6) and following (α7) this latter β strand (**Fig. 4a**). We will refer

to these dimers as canonical ones. Analysis of the interfaces within the Cest-2923 crystal with PISA [20] and PIC [21] web servers reveals that the contact region between monomers has an interface area of ~ 980 $Å^2$. The intermolecular contacts identified in this area are 26 H-bonds, 20 hydrophobic and aromatic-aromatic interactions and 2 salt bridges. Among the set of hydrogen bonds detected there are four between main chain atoms, which are those directly involved in the association between β8 strands (particularly, from residues Tyr225 and Leu227).

In addition, this same analysis revealed the existence of a second contact region between symmetry related molecules (molecules A-A and B-B) involving an even larger interface area (1460 $Å^2$). The assembly of Cest_Lp2923 monomers through the joint combination of these two contact regions renders a tetrameric structure made up of two canonical dimers, which is stable according to PISA (total buried area: 9780 $Å^2$; Gibb´s free energy of dissociation, ΔG^{diss}: 11.5 kcal mol^{-1}) (**Fig. 4b**). In this regard, it is worth to note that canonical dimers of close relatives of Cest-2923 such as EstE1 [15], Sto-Est [16], PestE [17], and Brefeldin A esterase [22] also form tetramers within the crystals ("canonical tetramers"), which nevertheless, are not comparable to the one observed for Cest-2923 (**Fig. 4c**). It is obvious that these observations raise the question of whether the Cest-2923 tetramers are crystallographic, i.e. by-product of the crystallization process. In this regard, results from different experimental approaches reveal a complex behaviour of Cest-2923: first, the crystal forms analysed by the structural genomics consortia (PDB entries 3d3n and 3bxp) reveal canonical dimers as the highest order oligomeric form within the crystals, what would support the crystallographic nature of the observed tetramers. In contrast to this, analyses of the oligomeric state of Cest-2923 in solution by analytical ultracentrifugation techniques (**Fig. 5**) reveals a complex scenario, which is consistent with an associative system involving monomeric, dimeric and tetrameric species. Thus, sedimentation velocity studies carried out in Tris buffer (20 mM Tris, pH 8.0, with 0.1 M NaCl) show that Cest-2923 behaves as (at least) two molecular species in solution, with sedimentation coefficients of 3.2 ± 0,2 S (n = 3) and 6.6 ± 0,1 S (n = 3), and estimated average molecular masses of 32 kDa and 96 kDa, respectively, which are values consistent with monomeric and trimeric Cest-2923 species (**Fig. 5a**). Considering the above crystallographic results, where dimers and tetramers have been observed for this protein, this scenario can be easily explained in terms of two association equilibria: a fast equilibrium (within the time scale of the sedimentation velocity

experiment, namely 6 hours) between dimers and tetramers, therefore explaining the average molecular mass of the 6.8 S species (intermediate between dimers and tetramers), and a second, slow equilibrium between monomers and dimers, therefore explaining the peak assignable to the monomer.

As expected from these latter ultracentrifugation results, sedimentation equilibrium experiments carried out under identical experimental conditions, fitted well to a monomer to tetramer association scheme, but also to an ideal model considering a unique species with an estimated average molecular mass of 69.8 ± 5.4 kDa (**Figs. 5b and 5c**) what would indicate that the system is mainly shifted to the dimeric species under neutral conditions. In this regard, it is worth to note that the two crystal forms prepared by the structural genomics consortia, where only canonical dimers were observed, were both obtained at pH 7.5 (PDB entry 3bxp: 30% 1,2-propanediol, 20% PEG 400, 0.1 M HEPES, pH 7.5; PDB entry 3d3n: 5% PEG 8000, 0.1 M calcium acetate, 0.1 M HEPES, pH 7.5).

Conversely, since the Cest-2923 crystals described in this work, which revealed the presence of tetramers, were obtained in 1.7 M ammonium sulphate, 0.15 M sodium acetate, pH 4.6, we also analysed the behaviour of the enzyme in solution at acidic conditions. Unexpectedly, we found that Cest-2923 precipitates in sodium acetate buffer (20 mM sodium acetate, pH 4.6 with 0.1 M NaCl) even at low protein concentration (0.2 mg/ml), but it was stable at pH 5.5. In this regard, both the far-UV CD spectrum at 25 ºC and the thermal denaturation curve measured in acetate buffer, pH 5.5 are indistinguishable from those registered at pH 8.0, indicating that there are no significant structural differences and changes in stability **(Fig. S2)**. Under these acidic conditions, sedimentation velocity analyses revealed a similar profile as those observed at pH 8.0, although with a relative lower contribution of the monomeric species for samples with the same protein concentration in comparable experiments (not shown). As expected, sedimentation equilibrium experiments fitted well to a monomer to tetramer associative model, and also to an ideal one with a unique species with an average molecular mass of 98.6 ± 0,6 kDa (**Figs. 5d and 5e**), indicating a displacement of the equilibria towards the tetrameric form relative to the neutral conditions.

Combining the results derived from these two distinct experimental approaches (crystallographic and analytical ultracentrifugation) we can deduce that Cest-2923 behaves in solution as an associative system well described by two equilibria, namely, a fast equilibrium between species with molecular

masses consistent with monomers and dimers and another, much faster one between dimeric and tetrameric species, and secondly that the crystallization process is an active player in selecting a pre-existing oligomeric form: dimers at neutral conditions, tetramers at acidic ones. Hence, we claim that the oligomeric forms determined by protein crystallography are not a mere crystallographic by-product but reveal intrinsic, associative properties of Cest-2923. Nevertheless, determination of the structural basis of the pH-dependence of the complex associative behaviour of Cest-2923 is not straightforward. Analysis of the interactions between Cest-2923 subunits with PISA [20] and PIC [21] revealed that the hydrophobic and H-bond interactions are the main driving force for protein association, mainly for dimer formation but also for tetramer formation. If this is the case, a displacement of the association equilibria towards tetramer formation can be predicted both under acidic or basic conditions with respect to the Cest-2923 isoelectric point (theoretical value: 6.5). In this sense, we carried out analytical ultracentrifugation studies of Cest-2923 at pH 9.0 (20 mM Tris, pH 9.0, 0.1 M NaCl) essentially as above (both sedimentation velocity and equilibrium assays). The obtained results (**Fig. S3**) are similar to those obtained under acidic conditions in agreement with an association process mainly guided by hydrophobic interactions.

As indicated above, EstE1 [15], Sto-Est [16], PestE [17], and Brefeldin A esterase [22] form canonical tetramers within the crystals (**Fig. 4c**). These tetramers have not been considered a crystallographic by-product since they were observed in different crystal lattices with crystals prepared in disparate conditions. It is worth to remark that this conclusion was derived despite these proteins were dimers in solution at much lower concentrations [17]. It is obvious that this behaviour resembles the one described here for Cest-2923 and therefore similar association equilibria for these proteins cannot be dismissed. From a structural viewpoint, Cest-2923 tetramers are not canonical ones, and are almost perfectly superimposable to those of the putative sugar hydrolase YeeB from *Lactococcus lactis* (PDB entry 3hxk), one of its closest structural relatives (**Fig. 4d**). When compared, it can be seen that both canonical and non canonical tetramers result from a head-to-head association since the same region from both canonical dimers is the one involved in association, although this region is different in both types of tetramers: thus, defining the *cis* face of the dimers as the one in which the C-terminal α-helix of the participating monomers is situated, non canonical tetramers would result from a *cis*-to-*cis* association whereas canonical ones would result from a *trans*-to-*trans* association. In both cases the final oligomer

exhibits a 222 point group although it is evident that the relative orientation of the dimers within tetramers is also different: if one dimer of each tetramer is fixed as a reference and is equally oriented for comparison the other dimers are rotated with respect to each other around 60º (**Fig. S4**).

As a whole, these results indicate that Cest-2923 displays a pleomorphic behaviour since it can form different oligomeric assemblies depending on pH, protein concentration and probably other environmental conditions as can be derived from crystallization experiments. We believe that this behaviour reflects an intrinsic property of the enzyme although on the other hand, we have no experimental basis to claim that this property has functional consequences *in vivo*. Undoubtedly, this needs to be further investigated.

Biochemical characterization

The most relevant enzymatic properties of Cest-2923 have been examined (**Fig. 6**). The optimum pH for hydrolytic activity against *p*-nitrophenyl acetate (see below) is 7.0 (**Fig. 6a**), which is a value typically observed for esterases, in contrast to the higher pH values (~ 8.0) displayed by lipases [23]. Regarding to temperature, the esterase presented highest activity at ~30 ºC, although at 45 ºC it exhibited a high level of activity (~65%) (**Fig. 6b**). These values for optimum pH and temperature are commonly found in other esterases from Lactobacilli [24-26]. On the other hand, temperature stability measurements show a drastic reduction in Cest-2923 hydrolytic activity upon incubation of the esterase at 55 ºC (**Fig. 6c**). This result agrees well with the analysis of protein thermostability carried out by far-UV CD spectroscopy, which revealed an apparent $T_{1/2}$ value around 60 ºC at neutral and acidic pH values **(Fig. S2)**.

The acyl-length selectivity against *p*-nitrophenyl ester substrates follows this order: C2 > C4 > C8 > C12 > C14, indicating a preference for short acyl-length esters (**Fig. 6d**). The kinetic parameters for C2 and C4 substrates were determined spectrophotometrically. In both cases, Cest-2923 exhibited a hyperbolic Michaelis-Menten kinetics (not shown). The kinetic parameters are shown in **Table 2**. From the values of these parameters it can be deduced that the catalytic efficiency (k_{cat}/K_m) for pNPA hydrolysis is around 75-fold the one observed for pNPB hydrolysis. Also, substrate specificity has been analysed with the use of a library of esters as described previously [27]. This study reveals maximum hydrolysis against phenyl acetate, which is considered as reference (100% activity), and also significant

activity (> 10% of the activity observed for phenyl acetate) against methyl bromoacetate and isopropenyl acetate. Within the limitations of the ester library employed, this result suggests a broader specificity for the alcohol part of the substrate and preference for small moieties for the acid part.

These three substrates were subsequently used for crystallographic studies with the aim to determine the structure of the corresponding complexes. With this purpose, native crystals were incubated for ~60 secs with a cryosolution containing the substrate at a concentration of 10 mM. Diffraction data recorded at beamline ID23-1 from the ESRF (Grenoble, France) with two types of these crystals (those prepared with methyl bromoacetate rapidly cracked) permitted to solve their structure, which unfortunately did not result in the structure of the complexes but unexpectedly provided evidences of catalysis occurring within the crystals. Thus, we observed that upon incubation with the corresponding cryosolution the space group of the native crystals ($P6_322$) changed: those crystals incubated with phenyl acetate became monoclinic (*C*2 space group) whereas those incubated with isopropenyl acetate changed to the *P*622 hexagonal space group. Interestingly, in both cases, the hexagonal packing was preserved and, in fact, indexing of the diffraction data identified the native unit cell and 622 point group what suggests that these changes in crystal symmetry result from the ordered incorporation of new molecules within the crystal lattice (see **Table 1**). One interesting observation is the presence in both types of crystals of an acetate molecule in the vicinity of the nucleophile Ser116, instead of a sulphate molecule which appeared in native crystals (**Fig. S5**). We believe this is remarkable since acetate by itself cannot replace sulphate in the active site as deduced from the native structure. We interpret this result as the substitution of sulphate by the corresponding substrate, which is further hydrolysed. After this step, the alcohol is released in contrast to the acetate molecule, which remains in the active site.

Materials and methods

Bacterial strains, plasmids and DNA manipulations

L. plantarum WCFS1 was grown in MRS medium at 30ºC without shaking [28]. *Escherichia coli* DH10B was used for all DNA manipulations and *E. coli* BL21 (DE3) was used for expression in pURI3-Cter vector [29]. *E. coli* strains were cultured in Luria-Bertani (LB) medium at 37ºC and 140 rpm.

The gene *lp_2923* from *L. plantarum* WCFS1 coding for Cest-2923 was cloned and overexpressed following a strategy previously described [30]. Briefly, the gene was PCR-amplified with HS Prime Start DNA polymerase (Takara) by using the primers 856 (TAACTTTAAGAAGGAGA TATACATatgcaagttgaacagcgcaca) and 857 (GCTATTAATGATGATGATGATGATGataattacc agctaacaatc) (the nucleotides pairing the expression vector sequence are indicated in uppercase characters, and the nucleotides pairing the *lp_2923* gene sequence are written in lowercase characters). The corresponding 831pb purified PCR product was inserted into the pURI3-Cter vector by using the restriction enzyme- and ligation-free cloning procedure to produce C-terminally His-tagged Cest-2923 essentially as described previously [30].

E. coli DH10B cells were transformed, recombinant plasmids were isolated, and those containing the correct insert were identified by restriction-enzyme analysis, verified by DNA sequencing, and then transformed into *E. coli* BL21 (DE3) cells.

Expression and purification of recombinant Cest-2923

Cells carrying the recombinant plasmid pURI3-Cter-lp_2923 were grown at 37 ºC in LB media containing ampicillin (100 µg/ml) and induced by adding 0.4 mM isopropyl-β-D-thiogalactopyranoside. After induction, the cells were grown at 22 ºC during 20 h and collected by centrifugation using a Beckman Coulter J-25 Avanti centrifuge (7500 x g for 15 min at 4 ºC). Cells were resuspended in 20 ml of 20 mM Tris-HCl, pH 8.0 containing 100 mM NaCl per liter of cell culture. Crude extracts were prepared by French Press lysis of cell suspensions. The lysate was centrifuged at 17,400 x g for 40 min at 4 ºC using a Beckman Coulter J-25 Avanti centrifuge.

The supernatant was filtered through a 0.22 µm filter (Millipore) and subsequently loaded onto a HisTrap-FF column previously equilibrated in binding buffer (20 mM Tris-HCl, pH 8.0 containing 100

mM NaCl and 10 mM imidazole). The recombinant His-tagged Cest-2923 was eluted with a linear gradient of imidazole (from 10 mM to 500 mM) with an ÄKTA Prime Plus. Fractions containing Cest-2923 were pooled and concentrated by ultrafiltration with a YM-10 membrane (Amicon). The protein (2 ml) was then loaded onto a HiLoad^{TM} 16/60 Superdex 200 prep-grade (GE Healthcare) equilibrated in Tris buffer (20 mM Tris-HCl, pH 8.0 containing 100 mM NaCl). The purity of the enzyme was checked by SDS-PAGE. Pure protein was finally concentrated to 10 mg/ml for crystallization trials by ultrafiltration and stored at -80 ºC until use.

Enzyme activity assay

Esterase activity was determined spectrophotometrically using *p*-nitrophenyl acetate as substrate. The rate of hydrolysis of *p*-NP acetate for 10 min at 30 ºC was measured in 50 mM sodium phosphate buffer pH 7.0 at 348 nm in a spectrophotometer (UVmini-1240 Shimadzu). The reaction was stopped by chilling on ice.

In order to carry out the reaction a stock solution of 25 mM of *p*-NP acetate was prepared in acetonitrile/isopropanol (1/4 *v/v*) [31] and mixed with 50 mM sodium phosphate buffer, pH 7.0 to obtain a substrate final concentration of 1 mM. Reaction was initiated by adding 10 µg of protein. Control reactions containing no enzyme were utilized to account for any spontaneous hydrolysis of the substrates tested. Enzyme assays were performed in triplicate. One unit of esterase activity was defined as the amount of enzyme required to release 1 µmol of *p*-nitrophenol per minute under the previously described conditions.

Substrate specificity

The substrate specificity of Cest-2923 was investigated with two different approaches: first, we studied the dependence of the hydrolytic activity of the enzyme on the aliphatic chain length of the substrates by using *p*-nitrophenyl (*p*-NP) esters with various chain lengths: *p*-NP acetate (C2); *p*-NP butyrate (C4); *p*-NP caprylate (C8); *p*-NP laurate (C12) and *p*-NP myristate (C14) essentially as described previously [10]. Briefly, a stock solution of each *p*-NP ester was prepared in acetonitrile/isopropanol (1/4 *v/v*). Substrates were emulsified to a final concentration of 0.5 mM in 50 mM sodium phosphate buffer, pH 7.0,

containing 1.1 mg/ml Arabic gum and 4.4 mg/ml Triton X-100. The reaction mix consisted of 990 µl of emulsified substrate and 10 µl of enzyme solution (10 µg of protein). Reactions were carried out at 30 ºC in a spectrophotometer (UVmini-1240 Shimadzu) as described above.

Second, substrate specificity was also analysed using the ester library described previously by Liu et al [9]. Briefly, the screening was performed in a 96-well plate Flat Bottom (Sarstedt) where final reaction volume was 200 µl and each well contained a different substrate (1 mM final concentration in 1 % acetonitrile). A buffer/indicator solution containing 0.44 mM of *p*-nitrophenol was used as pH indicator in 1 mM sodium phosphate buffer pH 7.2. Cest-2923 (10 µg in 20 µl of 1 mM sodium phosphate buffer pH 7.2) was added to each well and reactions were followed by measuring the decrease in absorbance at 410 nm for 2 h at 30ºC in a Synergy HT BioTek microplate spectrophotometer. Blanks without enzyme were carried out for each substrate and data were collected in triplicate.

The general ester library consisted of 50 commercially available esters. These were chosen to identify not only acyl chain length preferences of the hydrolases but also their ability to hydrolyse hindered or charged substrates. Simple alkyl esters as well as activated esters (vinyl and phenyl esters, esters with electron-withdrawing substituents in the acyl portion) were included to test whether activated esters would react faster.

Biochemical characterization of Cest-2923

In order to investigate temperature effect, reactions were performed in 50 mM sodium phosphate buffer (pH 7.0) at 4, 20, 30, 37, 40, 45, 55 and 65 ºC. Effect of pH was investigated by assaying esterase activity in a range of pH values from 5.5 to 9.0 at 30 ºC. Buffers used were acetic acid-sodium acetate buffer for pH 5.5, sodium phosphate buffer for pH 6-7, Tris-HCl buffer for pH 8 and glycine-NaOH buffer for pH 9. A 100 mM concentration was used in all the buffers. Although initially activity measurements were done at lower pH values (between 3.0 and 5.0) these are not reported since protein aggregation was detected in acetate buffer pH 4.6 or 5.0.

For temperature stability measurements, the recombinant esterase was incubated in 50 mM sodium phosphate buffer pH 7.0 at 20, 30, 37, 45, 55 and 65 ºC for 15 min, 30 min, and 1, 2, 3, 4, 6 and 20 h. After incubation, the residual activity was measured as described above.

Analytical ultracentrifugation

Equilibrium and sedimentation velocity ultracentrifugation experiments were performed at 10,500 rpm, 20ºC, using a Beckman XL-A ultracentrifuge with an An-50Ti rotor and standard double sector centerpiece cells. Solvent density (1.0029 mg/ml) and the partial specific volume of Cest-2923 (0.719) were calculated from the buffer composition (100 mM NaCl, 20 mM Tris-HCl or 100 mM NaCl, 20 mM sodium acetate) and from the predicted amino acid composition, respectively, with SEDNTERP [32]. Data from sedimentation velocity and equilibrium experiments were analysed using the programs Sedfit [33] and Heteroanalysis [34], respectively.

Circular dichroism spectroscopy

Far-UV circular dichroism (CD) measurements were carried out on a Jasco J-715 spectropolarimeter equipped with a thermostated cell holder and a Peltier temperature control accessory. The instrument was calibrated with (+)-10-camphorsulfonic acid. CD spectra were recorded in 0.1 cm path length quartz cell cuvettes from 250 to 205 nm, using a protein concentration of 6.4 μM (1 nm bandwidth, 4 s response, and 20 nm/min scan speed). Each spectrum herein presented is the average accumulation of four scans. Baseline subtraction was performed in all cases. Results are expressed as mean residue ellipticity $[\theta]_{MRW}$, in units of degree cm^2 $dmol^{-1}$ of amino acid (Mr = 110 for this protein). Thermal transitions were also analysed by CD spectroscopy by monitoring the variation of the ellipticity at 218 nm as the temperature was increased from 20 to 90 ºC at 50 ºC/h. The normalized ellipticity value at each temperature was calculated as $([\theta]_T-[\theta]_{25})/([\theta]_{90}-[\theta]_{25})$, where $[\theta]_T$ is the ellipticity value at temperature T, and $[\theta]_{25}$ and $[\theta]_{90}$ are the ellipticity values at 25 ºC and 90 ºC, respectively. Three different samples were analysed, although the traces shown correspond to individual samples.

Crystallization and data collection

Initial crystallization conditions for Cest-2923 were determined by the sitting-drop vapour diffusion method with commercial screens from Hampton Research (Riverside, California, USA) in Innovaplate

SD-2 96-well plates set up using a Nanodrop Innovadyne robot. Each drop contained 250 nl of protein (7 mg/ml) in Tris–HCl buffer (20 mM Tris–HCl pH 8.0 containing 0.1 M NaCl) and 250 nl of reservoir solution. Drops were equilibrated against 65 µl reservoir solution. Scaling up of the crystallization conditions using hanging drops in 24-well VDX plates (2:1 protein:precipitant volume ratio; total volume 3 µl) rendered high quality diffracting crystals in 1.7 M ammonium sulphate, 0.15 M sodium acetate, pH 4.6. Crystals suitable for X-ray analysis were transferred to an optimized cryoprotectant solution (reservoir solution plus 20% (*v/v*) 2-methyl-2,4-pentanediol) for ~10 secs and then cryocooled at 100 K in the cold nitrogen-gas stream. Diffraction data were recorded on a Pilatus 6M detector (Area Detector Systems Corp.) at beamline ID29 at the European Synchrotron Radiation Facility (ESRF) (Grenoble, France). Diffraction images were processed with XDS [35] and the data scaled and analysed using SCALA [36] from the CCP4 software suite [37]. Cryosoaking experiments were carried out with native Cest-2923 crystals, with a cryosolution containing phenyl acetate or isopropenyl acetate (10 mM final concentration. These new crystals were measured at beamline ID23-1 at the ESRF. Diffraction data were recorded on a Pilatus 6M-F detector (Area Detector Systems Corp.). Data statistics are summarized in **Table 1**.

Structure determination and refinement

The crystal structure of Cest-2923 was determined by the molecular replacement method with PHASER [38] using the PHENIX software suite [39]. The atomic coordinates of the enzyme deposited by the Northeast Structural Genomics Consortium (PDB code: 3d3n) were used as search model. Importantly, the 25-residue long loop containing the catalytic His233 residue not defined in this model could be modeled with the diffraction data obtained from the new crystal form described in this work. Conversely, the atomic model deposited by the Joint Center for Structural Genomics for Cest_Lest-2923 (PDB code: 3bxp) is discussed above. Restraint refinement and automatic water molecule placement was done with phenix-refine [40]. Stereochemical validation was carried out using the program MOLPROBITY [41]. The refinement statistics are summarized in **Table 1**. The final model has an R-factor of 15.5 % and an R_{free} of 19.5 %, and included 550 amino acid residues, 9 sulphate molecules, 3 acetate molecules, 1 Tris and 520 solvent molecules. Details on the structures derived from crystals soaked with substrates phenyl

acetate and isopropenyl acetate can be seen in **Table 1**. The PISA [20] and PIC [21] webservers were used to calculate values of buried interface areas. Ribbon diagrams were prepared using PyMOL [42].

Acknowledgements

We thank the ESRF (Grenoble, France) for provision of synchrotron radiation facilities (ID29 and ID23-1). JMM thanks Margarita Menéndez for her helpful advices on ultracentrifugation analyses. Financial support from the Ministerio de Economía y Competitividad (BFU2010-17929/BMC) and the Factoría de Cristalización (Consolider-Ingenio-2007) (to J.M.M.), AGL2011-22745 (to R. M.), FUN-C-FOOD Consolider 25506 (to R. M.) is greatly appreciated. Y.A., M.E-T. and I.A. and are recipients of the following fellowships: CSIC-CITMA, JAE Predoc (CSIC), FPU (MEC), respectively.

References

1. Bornscheuer UT (2002) Microbial carboxyl esterases: classification, properties and application in biocatalysis. *FEMS Microbiol Rev* **26**, 73-81.

2. Jaeger KE, Dijkstra BW & Reetz MT (1999) Bacterial biocatalysts: molecular biology, three-dimensional structures, and biotechnological applications of lipases. *Annu Rev Microbiol* **53**, 315-351.

3. Arpigny JL & Jaeger KE (1999) Bacterial lipolytic enzymes: classification and properties. *Biochem J* **343**, 177-183.

4. Hotelier T, Renault L, Cousin X, Negre V, Matchot P & Chatonnet A (2004) ESTHER, the database of the alpha/beta hydrolase fold superfamily of proteins. *Nucleic Acids Res* **32**: D145.

5. Holm C, Osterlund T, Laurell H & Contreras JA (2000) Molecular mechanisms regulating hormone-sensitive lipase and lipolysis. *Annu Rev Nutr* **20**, 365-393.

6. Ollis DL, Cheah E, Cygler M, Dijkstra B, Frolow F, Franken SM, Harel M, Remington SJ, Silman I, Schrag J, et al. (1992) The alpha/beta hydrolase fold. *Protein Eng* **5**, 197-211.

7. Nardini M & Dijkstra BW (1999) α/β hydrolase fold enzymes: the family keeps growing. *Curr Opin Struct Biol* **9**, 732-737.

8. Heikinheimo P, Goldman A, Jeffries C & Ollis DL (1999) Of barn owls and bankers: a lush variety of α/β hydrolases. *Structure* **7**, R141-R146.

9. Rodríguez H, Curiel JA, Landete JM, de las Rivas B, López de Felipe F, Gómez-Cordovés C, Mancheño JM & Muñoz R (2009) Food phenolics and lactic acid bacteria. *Int J Food Microbiol* **132**, 79-90.

10. Brod FCA, Vernal J, Bertoldo JB, Terenzi H & Arisi ACM (2010) Cloning, expression, purification, and characterization of a novel esterase from *Lactobacillus plantarum*. *Mol Biotechnol* **44**, 242-249.

11. Kleerebezem M, Boekhorst J, Kranenburg R, Molenaar D, Kuipers OP, Leer R, Tarchini R, Peters SA, Sandbrink HM, Fiers MWEJ, Stiekema W, Lankhorst RMK, Bron PA, Hoffer SM, Groot MNN, Kerkhoven R, de Vries M, Ursing B, de Vos WM & Siezen RJ (2003) Complete genome sequence of *Lactobacillus plantarum* WCFS1. *Proc Natl Acad Sci USA* **100**, 1990-1995.

12. Álvarez Y, Esteban-Torres M, Acebrón I, de las Rivas B, Muñoz R, Martínez-Ripoll M & Mancheño JM (2011) Preliminary X-ray analysis of twinned crystals of the Q88Y25_Lacpl esterase from *Lactobacillus plantarum. Acta Crystallog* F**67**, 1436-1439.

13. Hemilä H, Koivula TT & Palva I (1994) Hormone-sensitive lipase is closely related to several bacterial proteins, and distantly related to acetylcholinesterase and lipoprotein lipase: identification of a superfamily of esterases and lipases. *Biochim Biophys Acta* **1210**, 249-253.

14. Holm L & Rosenström P (2010) Dali server: conservation mapping in 3D. *Nucleic Acids Res* **38**, W545-W549.

15. Byun JS, Rhee JK, Kim ND, Yoon JH, Kim DU, Koh E, Oh JW & Cho HS (2007) Crystal structure of hyperthermophilic esterase Est1 and the relationship between its dimerization and thermostability properties. *BMC Struct Biol* **7**, 47-57.

16. Angkawidjaja C, Koga Y, Takano K & Kanaya S (2012) Structure and stability of a thermostable carboxylesterase from the thermoacidiphilic archaeon *Sulfolobus tokodaii*. *FEBS J* **279**, 3071-3084.

17. Palm GJ, Fernández-Álvaro E, Bogdanović X, Bartsch S, Sczodrok J, Singh RK, Böttchner D, Atomi H, Bornscheuer UT & Hinrichs W (2011) The crystal structure of an esterase from the hyperthermophilic microorganism *Pyrobaculum calidifontis* VA1 explains its enantioselectivity. *Appl Microbiol Biotechnol* **91**, 1061-1072.

18. De Simone G, Galdiero S, Manco G, Lang D, Rossi M & Pedone C (2000) A snapshot of a transition state analogue of a novel thermophilic esterase belonging to the family of mammalian hormone-sensitive lipase. *J Mol Biol* **303**, 761-771.

19. Zhu X, Larsen NA, Basran A, Bruce NC & Wilson IA (2003) Observation of an arsenic adduct in an acetyl esterase crystal structure. *J Biol Chem* **278**, 2008-2014.

20. Krissinel E & Henrick K (2007) Inference of macromolecular assemblies from crystalline state. *J Mol Biol* **372**, 774-797.

21. Tina KG, Bhadra R & Srinivasan N (2007) PIC, Protein Interactions Calculator. *Nucleic Acids Res* **35**, W473-W476.

22. Wei Y, Contreras JA, Sheffield P, Osterlund T, Derewenda U, Kneusel RE, Matern U, Holm C & Derewenda ZS (1999) Crystal structure of brefeldin A esterase, a bacterial homolog of the mammalian hormone-sensitive lipase. *Nature Struc Biol* **6**, 340-345.

23. Fojan P, Jonson PH, Petersen MTN & Petersen SB (2000) What distinguishes an esterase from a lipase: A novel structural approach. *Biochimie* **82**, 1033-1041.

24. Gobbeti M, Fox PF, Smacchi E, Stepaniak L & Damiani P (1996) Purification and characterization of a lipase from *Lactobacillus plantarum* 2739. *J Food Biochem* **20**, 227-246.

25. Fenster KM, Perkin KL & Steele JL (2003) Intracellular esterase from *Lactobacillus casei* LILA: nucleotide sequencing, purification and characterization. *J Dairy Sci* **86**, 1118-1129.

26. Gobbeti M, Fox PF, Smacchi E & Stepaniak L (1997) Isolation and characterization of a tributyrin esterase from *Lactobacillus plantarum* 2739. *J Dairy Sci* **80**, 3099-3106.

27. Liu AMF, Somers NA, Kazlauskas RJ, Brush TS, Zocher TS, Enzelberger MM, Bornscheuer UT, Horsman GP, Mezzetti A, Schmidt-Dannert C & Schmid RD (2001) Mapping the substrate selectivity of new hydrolases using colorimetric screening: lipases from *Bacillus thermocatenolatus* and *Ophiostoma piliferum*, esterases from *Pseudomonas fluorescens* and *Streptomyces diastatochromogenes*. *Tetrahedron Asym* **12**, 545-556.

28. De Man JC, Rogosa M & Sharpe ME (1960) A medium for the cultivation of lactobacilli. *J Appl Bacteriol* **23,** 130−135.

29. Curiel JA, de las Rivas B, Mancheño JM & Muñoz R (2011) The pURI family of expression vectors: A versatile set of ligation independent cloning plasmids for producing recombinant His-fusion proteins. *Prot Express Purif* **76**, 44–53.

30. De las Rivas B, Curiel JA, Mancheño JM & Muñoz, R (2007) Expression vectors for enzyme restriction- and ligation-independent cloning for producing recombinant His-fusion proteins *Biotechnol. Prog* **23**, 680–686.

31. Glogauer A, Martini VP, Faoro H, Couto GH, Müller-Santos M, Monteiro RA, Mitchel DA, de Souza EM, O Pedrosa F & Krieger N (2011) Identification and characterization of a new true lipase isolated through metagenomic approach. *Microbial Cell Factories* **10**, 54.

32. Laue TM, Shah BD, Ridgeway TM & Pelletier SL (1992) *Biochemistry and Polymer Science.* Royal Society of Chemistry, London.

33. Schuck P (2000) Size distribution analysis of macromolecules by sedimentation velocity ultracentrifugation and Lamm equation modeling. *Biophys J* **78**, 1606-1619.

34. Cole JL & Lary JW (2009) *HeteroAnalysis*. Bioservices Center. University of Connecticut, Storrs, CT, Analytical Ultracentrifugation Facility.

35. Kabsch W (2010) XDS. *Acta Crystallog D Biol Crystallog* **66**, 125-132.

36. Evans PR (2011) An introduction to data reduction: space-group determination, scaling and intensity statistics. *Acta Crystallog D Biol Crystallog* **67**, 282-292.

37. Winn MD, Ballard CC, Cowtan KD, Dodson KD, Emsley P, Evans PR, Keegan RM, Krissinel EB, Leslie AGW, McCoy A, McNicholas SJ, Murshudov GN, Pannu NS, Potterton EA, Powell HR, Read RJ, Vagin A & Wilson KS (2011) Overview of the CCP4 suite and current developments. *Acta Crystallog D Biol Crystallog* **67**, 235-242.

38. McCoy AJ, Grosse-Kunstleve RW, Adams PD, Winn MD, Storoni LC & Read RJ (2007) Phaser crystallographic software. *J Appl Cryst* **40**, 658-674.

39. Adams PD, Afonine PV, Bunkóczi G, Chen VB, Davis IW, Echols N, Headd JJ, Hung LW, Kapral GJ, Grosse-Kunstleve RW, McCoy AJ, Moriarty NW, Oeffner R, Read RJ, Richardson DC, Richardson JS, Terwilliger TC & Zwart PH (2010) PHENIX: a comprehensive Python-based system for macromolecular structure solution. *Acta Crystallog D Biol Crystallog* **66**, 213-221.

40. Afonine PV, Grosse-Kunstleve RW, Echols N, Headd JJ, Moriarty NW, Mustyakimov M, Terwilliger TC, Urzhumtsev A, Zwart PH & Adams PD. (2012) Towards automated crystallographic structure refinement with phenix.refine. *Acta Crystallogr D Biol Crystallogr* **68**, 352-367

41. Chen VB, Arendall III WB, Headd JJ, Keedy DA, Immormino RM, Kapral GJ, Murray LW, Richardson JS & Richardson DC (2010) MolProbity: all-atom structure validation for macromolecular crystallography. *Acta Crystallogr D Biol Crystallogr* **66**, 12-21.

42. DeLano WL (2008) *The PyMOL Molecular Graphics System* (http://www.pymol.org).

Figure legends

Fig. 1. Amino acid sequence alignment of Cest-2923 with its closest homologs. Cest-2923 shares 33% and 32% sequence identity with the putative sugar hydrolase YeeB from *Lactococcus lactis* and the carboxylesterase lp_1002 from *Lactobacillus plantarum*, respectively. Colour code indicates: *blue*, conserved amino acid residues; *yellow*, similar residues; *red*, residues forming the catalytic triad in YeeB and lp_1002.

Fig. 2. Overall fold of the Cest-2923 subunit from *Lactobacillus plantarum* WCFS1. The tertiary structure of the Cest-2923 subunit fits the canonical α/β hydrolase fold where a central eight-stranded β-sheet (shown in *green*) is surrounded by five α-helices (*orange*). Two orthogonal views of the protein subunit are shown.

Fig. 3. Catalytic triad machinery of the Cest-2923 subunit from *Lactobacillus plantarum* WCFS1. (A) Stereo view of the catalytic triad environment of Cest-2923. Residues of the catalytic triad (Ser116, His233, Asp201) are shown as *orange sticks* and those participating in hydrogen bonding interactions as *grey sticks*; potential H-bonds are indicated as *black*, *broken* lines. A conserved water molecule that interacts with Asp201, which is conserved within the HSL family of enzymes, is shown as a *blue* sphere. (B) Stereo view of the surroundings of the sulphate molecule found in the active site of Cest-2923. The electron density map ($2F_o$-F_c in *blue*; contoured at 1-σ level) for the sulphate is shown. Residues of the catalytic triad are shown as *light yellow sticks.* Distances are given in Å.

Fig. 4. Dimeric and tetrameric assemblies of Cest-2923 from *Lactobacillus plantarum* WCFS1. (A) Canonical dimer of Cest-2923. The association of the subunits involves interactions between strands β8 and α-helices α6 and α7. The two subunits are shown in different colours. (B) Non-canonical tetramer of Cest-2923. The contacting region between canonical dimers is mainly formed by α-helix α1, the contacting loops between strands β2 and β3 and between strand β8 and α-helix α7 and the C-terminal

end. The four subunits are shown in different colours. (C) Canonical tetramer of HSL esterases. As an example it is shown the tetramer of the hyperthermophilic esterase EstE1 (PDB entry: 2c7b) [15]. Further details on the comparison between canonical and non-canonical tetramers can be found in Fig. S3. (D) Three dimensional superposition between the non-canonical tetramers of Cest-2923 (in transparent, *grey* cartoons) and those found for the putative sugar hydrolase YeeB from *Lactococcus lactis* (PDB entry 3hxk).

Fig. 5. Analytical ultracentrifugation analysis of Cest-2923 at neutral and acidic conditions. (A) Sedimentation coefficient *c*(*s*) distributions for Cest-2923 (13 μM) in Tris buffer (20 mM Tris-HCl, pH 8.0 with 0.1 M NaCl). Raw sedimentation velocity profiles for this analysis were acquired using absorbance at 280 nm, 45,000 rpm, 20 ºC, and different times (not shown). Calculations were done with the program SEDFIT [33]. (B) Sedimentation equilibrium analysis of Cest-2923 (13 μM) in Tris buffer (20 mM Tris-HCl, pH 8.0 with 0.1 M NaCl) at 12,000 rpm (*open* circles) and 17,300 (*open* squares). Absorbance at 280 nm is plotted against the radial position from the centre of the rotor. The fit to the data set (*solid line curves*) corresponds to a monomer-tetramer association equilibrium. Residuals from this fit are shown in the inset. (C) As the previous panel, but the fit corresponds to an ideal species. The best-fit weight average molecular mass is 69.8 ± 5.4 kDa. (D) Sedimentation equilibrium analysis of Cest-2923 (13 μM) in acetate buffer (20 sodium acetate, pH 5.5 with 0.1 M NaCl) at 13,400 rpm (*open* circles) and 19,500 (*open* squares). Other experimental conditions are identical to those at neutral conditions. The fit to the data set (*solid line curves*) corresponds to a monomer-tetramer association equilibrium. Residuals from this fit are shown in the inset. (E) As panel (D), but the fit corresponds to an ideal species. The best-fit weight average molecular mass is 98.6 ± 0,6 kDa.

Fig. 6. Biochemical characterization of Cest-2923 from *Lactobacillus plantarum* WCFS1. (A) Dependence on pH of hydrolytic activity of Cest-2923 against *p*-nitrophenyl acetate. *Open squares* indicate measurements in Tris buffer (pH 7.0) and phosphate buffer (pH 8.0) carried out to discard buffer-specific side effects. (B) Dependence on temperature of hydrolytic activity of Cest-2923 against *p*-

nitrophenyl acetate. The optimum temperature for esterase activity was ~30 ºC. (C) Analysis of the temperature stability of Cest-2923. Recombinant esterase was incubated in 50 mM sodium phosphate buffer pH 7.0 at 20 (*open circles*), 30 (*closed circles*), 37 (*open squares*), 45 (*closed squares*), 55 (*open triangles*) and 65 ºC (*closed triangles*) for 15 min, 30 min, and 1, 2, 3, 4, 6 and 20 h. In all cases, the values shown are the mean average of three independent experiments. (D) Dependence of the esterase activity of Cest-2923 on the aliphatic chain length of *p*-nitrophenyl (*p*-**NP**): *p*-**NP** acetate (C2); *p*-**NP** butyrate (C4); *p*-**NP** caprylate (C8); *p*-**NP** laurate (C12) and *p*-**NP** myristate (C14).

Table 1. Data Collection and Refinement Statistics

	Cest-2923	Cest-2923-PA	Cest-2923-IPA
PDB accession code	**4BZW**	**4C01**	**4BZZ**
Data collection			
Beamline	ID29 (ESRF)	ID23-1 (ESRF)	ID23-1 (ESRF)
Wavelength (Å)	0.9400	0.9687	0.9687
Space group	$P6_322$	$C2$	$P622$
Unit-cell parameters (Å)	$a = b = 141.65$, $c = 165.74$ $\alpha = \beta = 90^o$, $\gamma = 120^o$	$a = 244.9$, $b = 141.4$, $c = 82.69$ $\alpha = \gamma = 90^o$, $\beta = 90.0^o$	$a = b = 141.72$, $c = 82.29$ $\alpha = \beta = 90^o$, $\gamma = 120^o$
Resolution range (Å)	46.37-2.15	49.20-2.30	48.97-2.99
No. of measured reflections	1,051,757	509,575	74,713
No. of unique reflections[a]	53,876 [5,215]	124,688 [12,482]	9,994 [1,306]
Mean I/σ(I)[a]	17.2 [6.2]	143.2 [46.5]	13.7 [4.1]
Completeness (%)[a]	99.9 [98.8]	99.9 [100]	99.6 [98.9]
Redundancy[a]	19.5 [18.0]	4.1 [4.3]	7.5 [7.3]
R_{merge} (%)[a]; R_{pim} (%)[a]	13.3 [51.4]; 3.1 [12.4]	14.3 [66.1]; 13.6 [60.9]	11.9 [47.1]; 4.6 [18.5]
Wilson B factor (Å^2)	21.2	21.2	41.98
Molecules/non-H atoms			
Protein	2/4,332	6/12,897	1/2,144
Water	503/503	1,014/1,014	4/4
Sulphate	9/45	8/40	4/20
Acetate	3/12	6/24	3/12
Other molecules	1/8	17/86	1/3
Refinement			
R_{work}(%)/R_{free}(%)	15.5/19.5	22.5/27.9	15.6/21.4
Average B-factors (Å^2); protein	27.0	41.0	49.7
Average B-factors (Å^2); water	39.1	38.7	45.2
Average B-factors (Å^2); other	76.0	64.8	94.2
rms deviation bond length (Å)	0.007	0.008	0.008
rms deviation Angles (°)	1.000	1.160	1.060
Molprobity			
Ramachandran favoured (%)	97.0	92.0	95.0
Ramachandran outliers (%)	0.0	0.3	0.0

[a]Values for the highest resolution shell are given in brackets.

Table 2. Kinetic parameters for pNPA and pNPB hydrolysis by Cest-2923.

Substrate	V_{max} (μmol min^{-1} mg^{-1})	K_m (mM)	k_{cat} (s^{-1})	k_{cat}/ V_{max} (s^{-1} mM^{-1})
pNPA	660 ± 50	1.7 ± 0.2	343.6 ± 26	202 ± 28
pNPB	40 ± 8	7.6 ± 1.2	20.8 ± 4	2.7 ± 0.7

Enzyme activities were determined at 30 ºC in 50 mM sodium phosphate buffer, pH 7.0. Results are the mean value ± SD from three independent experiments.

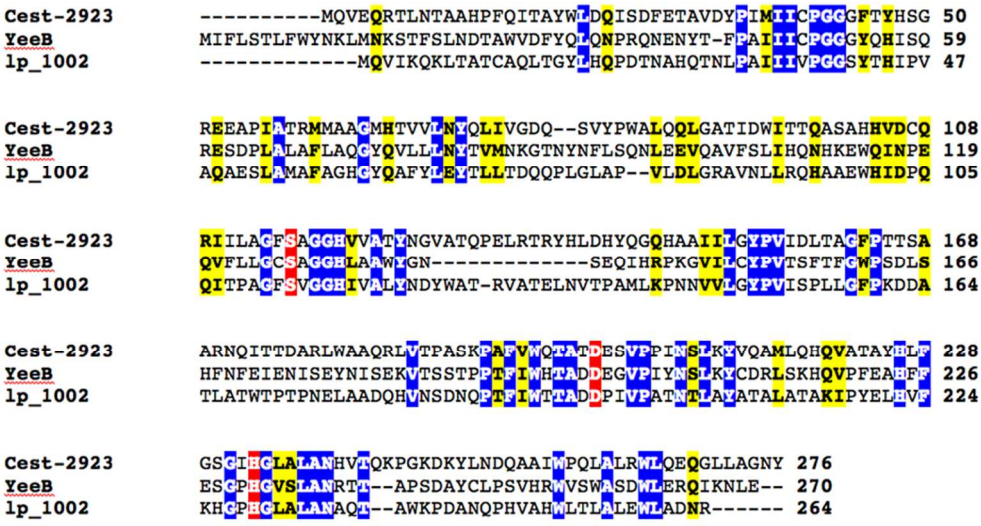

80x44mm (300 x 300 DPI)

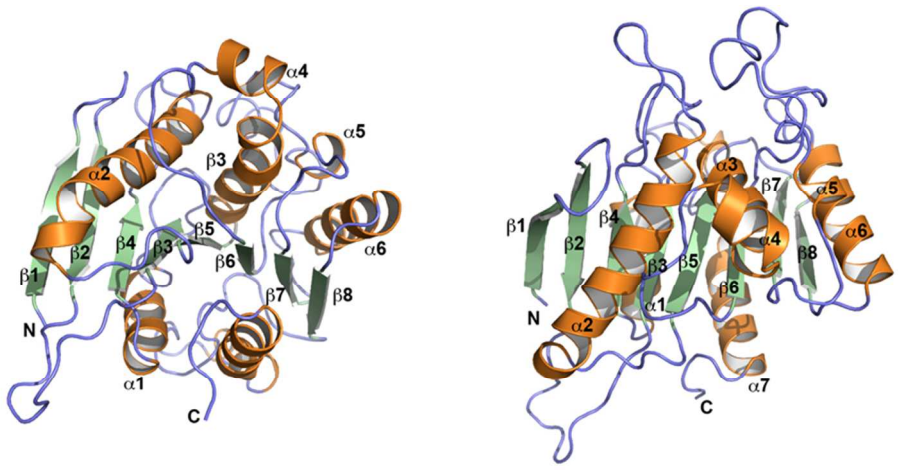

80x37mm (300 x 300 DPI)

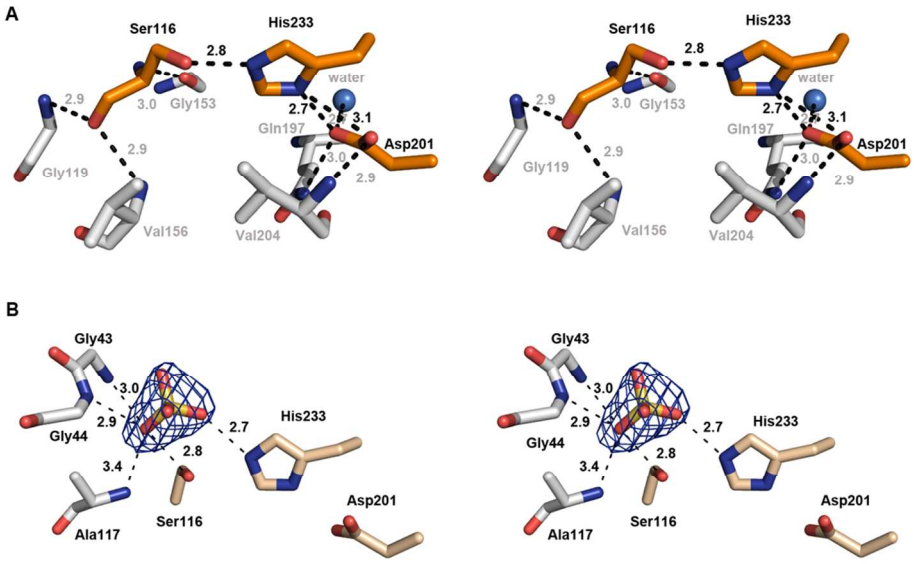

104x62mm (300 x 300 DPI)

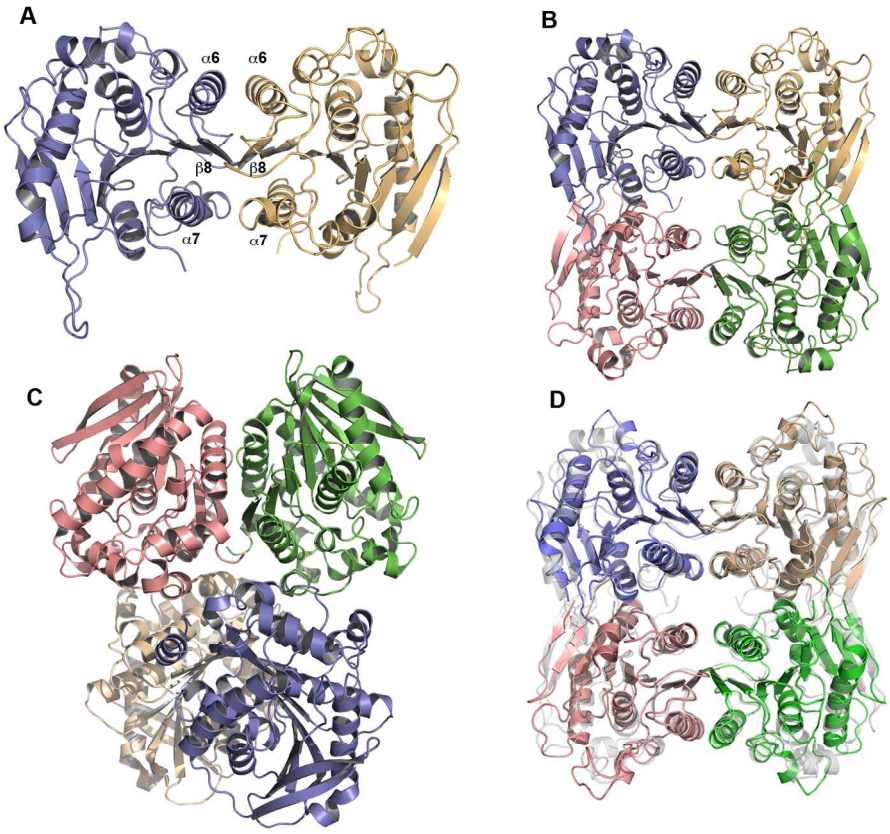

165x165mm (300 x 300 DPI)

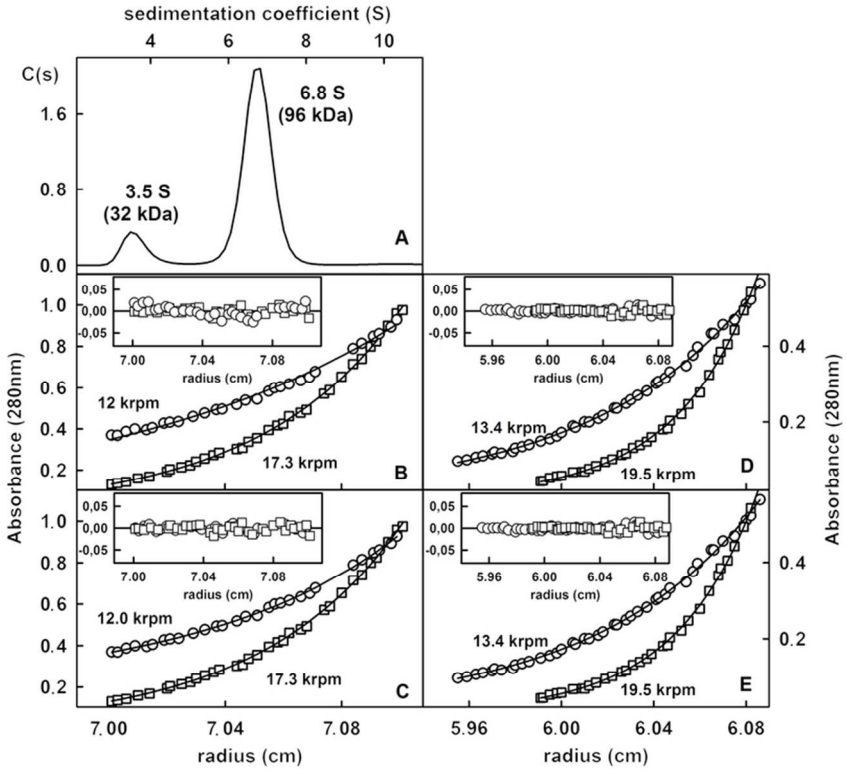

81x62mm (300 x 300 DPI)

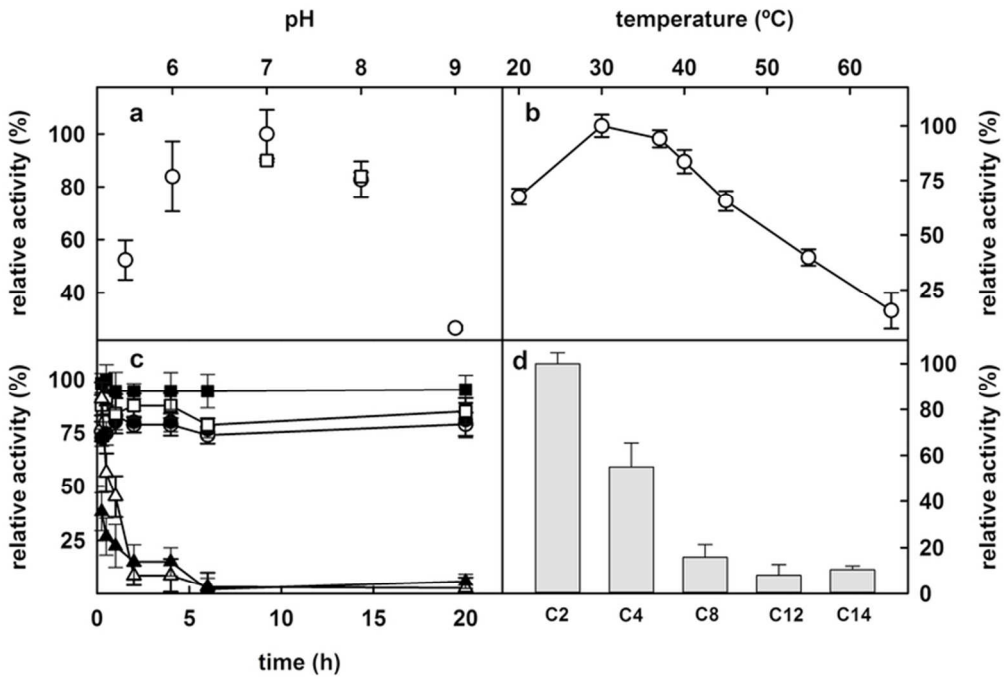

70x47mm (300 x 300 DPI)

Table 1. Data Collection and Refinement Statistics

	Cest-2923	Cest-2923-PA	Cest-2923-IPA
PDB accession code	**4BZW**	**4C01**	**4BZZ**
Data collection			
Beamline	ID29 (ESRF)	ID23-1 (ESRF)	ID23-1 (ESRF)
Wavelength (Å)	0.9400	0.9687	0.9687
Space group	$P6_322$	$C2$	$P622$
Unit-cell parameters (Å)	$a = b = 141.65$, $c = 165.74$ $\alpha = \beta = 90^o$, $\gamma = 120^o$	$a = 244.9$, $b = 141.4$, $c = 82.69$ $\alpha = \gamma = 90^o$, $\beta = 90.0^o$	$a = b = 141.72$, $c = 82.29$ $\alpha = \beta = 90^o$, $\gamma = 120^o$
Resolution range (Å)	46.37-2.15	49.20-2.30	48.97-2.99
No. of measured reflections	1,051,757	509,575	74,713
No. of unique reflections[a]	53,876 [5,215]	124,688 [12,482]	9,994 [1,306]
Mean $I/\sigma(I)$[a]	17.2 [6.2]	143.2 [46.5]	13.7 [4.1]
Completeness (%)[a]	99.9 [98.8]	99.9 [100]	99.6 [98.9]
Redundancy[a]	19.5 [18.0]	4.1 [4.3]	7.5 [7.3]
R_{merge} (%)[a]; R_{pim} (%)[a]	13.3 [51.4]; 3.1 [12.4]	14.3 [66.1]; 13.6 [60.9]	11.9 [47.1]; 4.6 [18.5]
Wilson B factor (Å^2)	21.2	21.2	41.98
Molecules/non-H atoms			
Protein	2/4,332	6/12,897	1/2,144
Water	503/503	1,014/1,014	4/4
Sulphate	9/45	8/40	4/20
Acetate	3/12	6/24	3/12
Other molecules	1/8	17/86	1/3
Refinement			
R_{work}(%)/R_{free}(%)	15.5/19.5	22.5/27.9	15.6/21.4
Average B-factors (Å^2); protein	27.0	41.0	49.7
Average B-factors (Å^2); water	39.1	38.7	45.2
Average B-factors (Å^2); other	76.0	64.8	94.2
rms deviation bond length (Å)	0.007	0.008	0.008
rms deviation Angles (º)	1.000	1.160	1.060
Molprobity			
Ramachandran favoured (%)	97.0	92.0	95.0
Ramachandran outliers (%)	0.0	0.3	0.0

[a]Values for the highest resolution shell are given in brackets.

Table 2. Kinetic parameters for pNPA and pNPB hydrolysis by Cest-2923.

Substrate	V_{max} (μmol min^{-1} mg^{-1})	K_m (mM)	k_{cat} (s^{-1})	k_{cat}/ V_{max} (s^{-1} mM^{-1})
pNPA	660 ± 50	1.7 ± 0.2	343.6 ± 26	202 ± 28
pNPB	40 ± 8	7.6 ± 1.2	20.8 ± 4	2.7 ± 0.7

Enzyme activities were determined at 30 ºC in 50 mM sodium phosphate buffer, pH 7.0. Results are the mean value ± SD from three independent experiments.

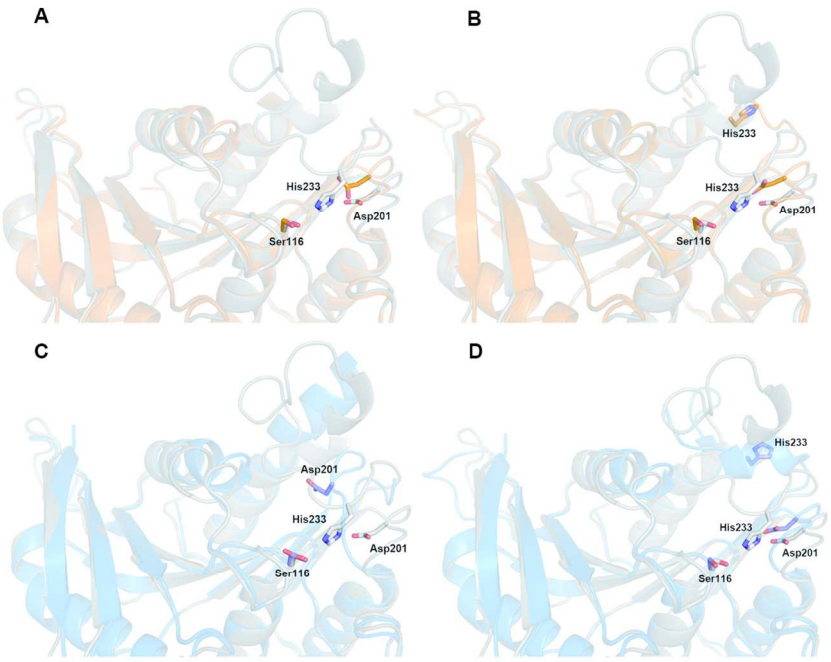

Fig. S1. Three dimensional superposition of the Cest-2923 model (chain A) from this work (shown as *grey cartoon*; PDB entry: 4bzw) with: (A) chain A, (B) chain B of PDB entry 3d3n deposited by the Northeast Structural Genomics Consortium (shown as *orange cartoon*), and (C) chain A, (D) chain B of PDB entry 3bxp deposited by the Joint Center for Structural Genomics (shown as *blue cartoon*). In all models, amino acid residues of each model from the catalytic triad are shown as *sticks* with the same colour code as the *cartoon* models.

109x150mm (300 x 300 DPI)

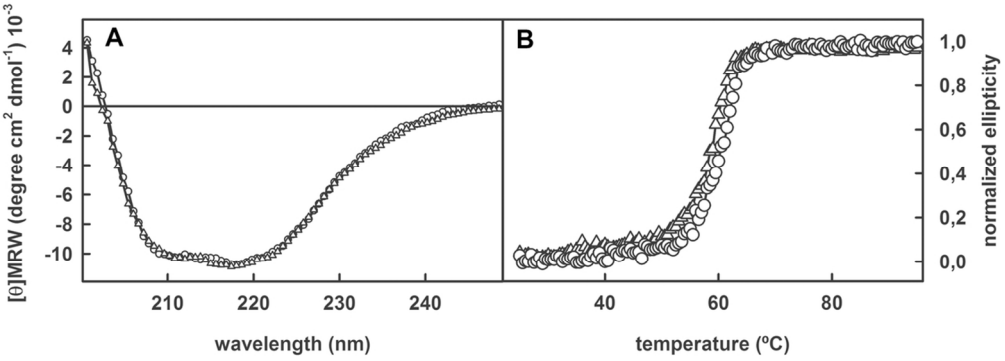

Fig. S2. (A) Far-UV CD spectra of Cest-2923 from *Lactobacillus plantarum* WCFS1 at neutral (20 mM Tris-HCl, pH 8.0 with 0:1 M NaCl) (open circles) and acidic (20 mM sodium acetate, pH 5.5 with 0.1 M NaCl) (open triangles) conditions. Protein concentration was 6.5 μM (0.2 mg/ml). (B) Heat denaturation curves for Cest-2923 in the same experimental conditions as in panel A (see Materials and Methods).

108x71mm (300 x 300 DPI)

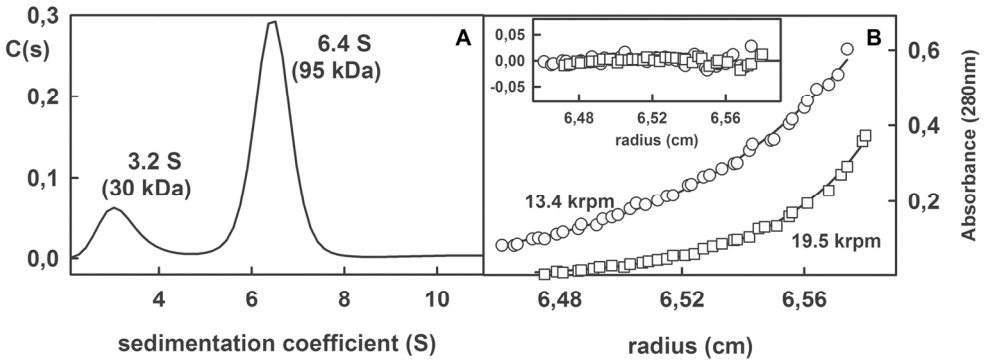

Fig. S3. Analytical ultracentrifugation analysis of Cest-2923 at basic conditions. (A) Sedimentation coefficient *c(s)* distributions for Cest-2923 (13 μM) in Tris buffer (20 Tris-HCl, pH 9.0 with 0.1 M NaCl). Raw sedimentation velocity profiles for this analisys were acquired using absorbance at 280 nm, 45,000 rpm, 20 ºC, and different times (not shown). Calculations were done with the program SEDFIT [33]. (B) Sedimentation equilibrium analysis of Cest-2923 (13 μM) in Tris buffer (20 mM Tris-HCl, pH 9.0 with 0.1 M NaCl) at 13,400 rpm (*open circles*) and 19,500 rpm (*open squares*). Absorbance at 280 nm is plotted against the radial position from the centre of the rotor. The fit to the data set (*solid line curves*) corresponds to a monomer-tetramer association equilibrium. Residuals from this fit are shown in the inset.

155x152mm (300 x 300 DPI)

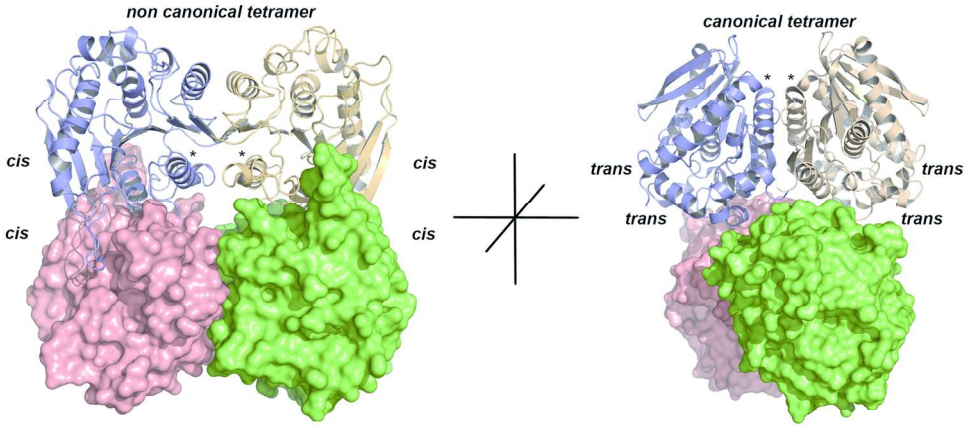

Fig. S4. Comparison between non-canonical and canonical tetramers. *Left*, non-canonical tetramer of Cest-2923. Subunits of one dimer are shown as *cartoon* models in *blue* and *wheat* colours, and the others from the accompanying dimer are shown as *surface* (*salmon* and *green*). Asterisks indicate the approximate position of the C-terminal α-helix, which defines the *cis* face of the subunits (see the text). *Right*, canonical tetramer of the hyperthermophilic esterase EstE1 (PDB entry: 2c7b) [15]. The colour code is the same as in the non-canonical tetramer of Cest-2923. The reference lines indicate the two-fold symmetry axes characteristic of both assemblies, i.e., they exhibit a 222 point group symmetry.

160x149mm (300 x 300 DPI)

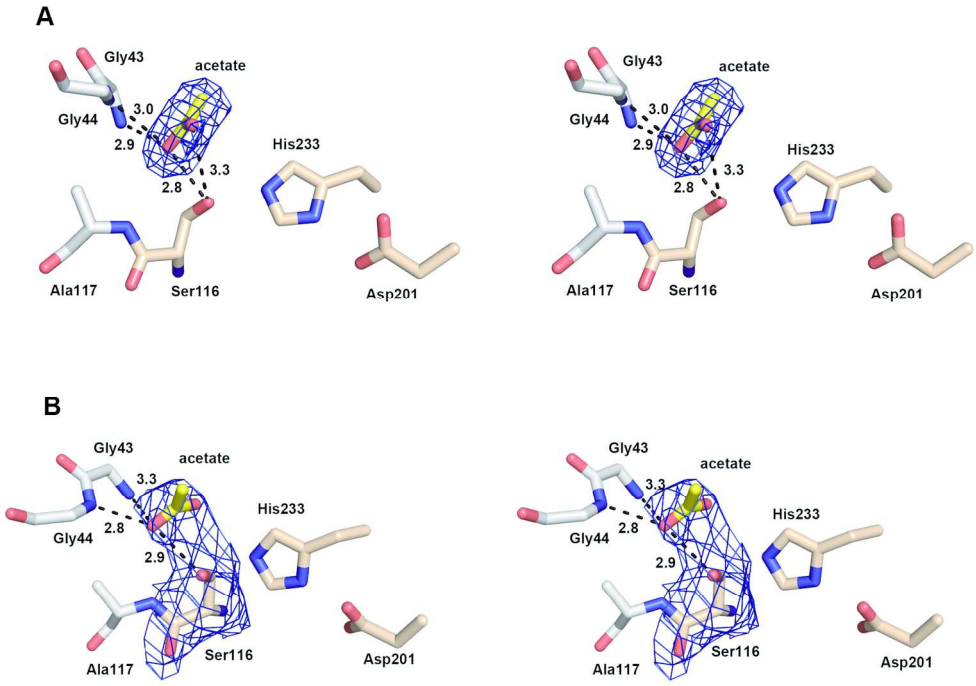

Fig. S5. Acetate molecule close to the nucleophile Ser116 in crystals soaked with the substrates phenyl acetate (PDB entry: 4c01) (A) or isopropenyl acetate (PDB entry: 4bzz) (B). Stereo views have been prepared in both cases. Hydrogen bonds involving the acetate molecule are shown as *black, broken lines*. Residues of the catalytic triad are shown as *sticks* in *wheat* colour. Other residues are shown as *grey*, *sticks*. The composite map calculated with *SFCHECK* (*2Fo - Fc* in *blue*; contoured at 1-σ level) is shown around the acetate molecule and the nucleophile. Distances are given in Å.

165x180mm (300 x 300 DPI)

Structure, biochemical characterization and analysis of the pleomorphism of carboxylesterase Cest-2923 from *Lactobacillus plantarum* WCFS1

Rocío Benavente[1], María Esteban-Torres[2], Iván Acebrón[1], Blanca de las Rivas[2], Rosario Muñoz[2], Yanaisis Álvarez[1] and José Miguel Mancheño[1]

1 Department of Crystallography and Structural Biology, Institute of Physical Chemistry Rocasolano, CSIC, Serrano 119, E-28006 Madrid, Spain

2 Laboratory of Bacterial Biotechnology, Institute of Food Science and Technology and Nutrition (ICTAN), CSIC, Juan de la Cierva 3, E-28006 Madrid, Spain

Keywords

α/β hydrolase; analytical ultracentrifugation; esterase; pleomorphism; X-ray crystallography

Correspondence

J.M. Mancheño, Department of Crystallography and Structural Biology, Institute of Physical Chemistry Rocasolano, CSIC, Serrano 119, E-28006 Madrid, Spain

Tel: +34-917459547

Fax: +34-5642431

E-mail: xjosemi@iqfr.csic.es

Running title

Structure and associative behaviour of Cest-2923.

Abbreviations

Cest-2923, carboxylesterase from *Lactobacillus plantarum* coded by gene *lp_2923*; HSL, hormone-sensitive lipase; LAB, lactic acid bacteria

Database

The atomic coordinates and structure factors have been deposited in the Protein Data Bank with accession numbers: **4BZW** for Cest-2923 from native crystals not soaked with substrates ($P6_322$ space group); **4C01** for Cest-2923 from crystals soaked with phenyl acetate ($C2$ space group); **4BZZ** for Cest-2923 from crystals soaked with isopropenyl acetate ($P622$ space group)

Abstract

The α/β hydrolase fold is one of the most versatile structures in the protein realm according to the diversity of sequences adopting such a three dimensional architecture. Here, we report the crystal structure of the carboxylesterase Cest-2923 from the lactic acid bacterium *Lactobacillus plantarum* WCFS1 refined to 2.1 Å resolution, determined its main biochemical characteristics and also carried out an analysis of its associative behaviour in solution. We found that the versatility of a canonical α/β-hydrolase fold, the basic framework of the crystal structure of Cest-2923, also extends to its oligomeric behavior in solution. Thus, we discovered that Cest-2923 exhibits a pH-dependent pleomorphic behaviour in solution involving monomers, canonical dimers and tetramers. Whereas at neutral pH the system is mainly shifted to dimeric species, at acidic conditions tetrameric species predominate. Interestingly, despite that these tetramers result from the association of canonical dimers, as commonly found in many other carboxylesterases from the hormone-sensitive lipase family, they can be defined as "non canonical" since they represent a different association mode. We identified this same type of tetramers in the closest relative of Cest-2923 structurally characterized, the sugar hydrolase YeeB from *Lactococcus lactis*. Interestingly, the observed associative behaviour is consistent with different crystallographic results of Cest-2923 from structural genomics consortia. Finally, we benefit from the presence of sulphate or acetate molecules (depending on the crystal form analysed) in the close vicinity of the nucleophile Ser116, to identify interactions with the putative oxyanion hole and also to deduce the existence of hydrolytic activity within Cest-2923 crystals.

Introduction

Carboxylesterases (EC 3.1.1.1) are enzymes widely distributed in animals, plants and microorganisms [1] that hydrolyse (synthesize) carboxylic esters. Specifically, the term carboxylesterase is adopted for enzymes acting on soluble, monomeric (e.g. below their critical micellar concentration) substrates, in contrast to lipases (EC 3.1.1.3), which display maximal activity against water-insoluble substrates [2, 3]. Based on their amino acid sequences and in particular in the presence of specific sequence motifs esterases and lipases are classified into four blocks, C, H, L and X [4]. Block H includes the plant carboxylesterase and hormone-sensitive lipase (HSL) families. The members of this latter family are distributed over all kingdoms of life and share sequence similarity to mammalian HSL [5]. Family IV of a previous classification of bacterial lipolytic enzymes [3] corresponds to the bacterial members of the HSL family.

Structurally, carboxylesterases belong to the α/β hydrolase superfamily of enzymes [6-8]. The crystal structures currently determined for members of this superfamily (524 PDB entries using the term α/β hydrolase fold from the SCOP classification) reveal a highly conserved protein architecture, the α/β hydrolase fold, a central, mostly parallel β-sheet, surrounded on both sides by α–helices. In all cases, the catalytic machinery is based on a highly conserved catalytic triad made up of a nucleophile (serine), an acid (Asp/Glu) and a histidine. The nucleophile is located in the so-called nucleophile elbow [8], which together with the "oxyanion hole" involved in the stabilization of the negatively charged tetrahedral intermediates, are the hallmarks of the α/β hydrolases.

One remarkable feature of the α/β hydrolase fold is its structural versatility: on the one hand, sequences with very low level of similarity (< 20 %) adopt essentially the same structural core and, on the other, it means that large domains can be added to this fold, which remains as an easily identifiable, conserved core. Usually these new domains are inserted between the canonical strands β6 and β7 and are believed to modulate specific properties of the enzyme [7,8].

Although lactic acid bacteria (LAB) play an important role in the production of fermented food products [9], little information exists about LAB as a source of enzymes [10]. In this regard, the recently reported genome of *Lactobacillus plantarum* WCFS1 [11] reveals the existence of numerous ORFs

coding putative esterases, among them the gene coding for the putative carboxylesterase Cest-2923 (*lp_2923)*. This enzyme has been recently crystallized by two independent structural genomics consortia (Joint Center for Structural Genomics, JCSG, and NorthEast Structural Genomics Consortium, NESG), which reported incomplete models for the enzyme (PDB entries: 3bxp for JCSG and 3d3n for NESG), which as revealed herein show features in conflict with the presence of the canonical catalytic triad.

Here, we report the complete crystal structure of Cest-2923, which as expected from sequence comparisons and the structural data from the above structural genomics consortia, exhibits a canonical α/β hydrolase fold. In addition, our biophysical studies reveal that the enzyme shows complex pH-dependent pleomorphic behaviour in solution. Finally, we have determined the main biochemical features of Cest-2923, which demonstrate that the enzyme is a true carboxylesterase as expected from the genome annotation.

Results and discussion

General comments about search models and description of the monomer structure

N-terminally His-tagged Cest-2923 when overexpressed using the pURI3-TEV vector as in our previous structural studies [12] turned out to be marginally stable in solution and therefore not suitable for crystallization experiments. On the contrary, the C-terminally His-tagged variant behaved well in solution and was suitable for crystallization. The enzyme crystallized in the hexagonal space group $P6_322$ (unit-cell dimensions $a = b = 141.65$ Å, $c = 165.74$ Å, $\alpha = \beta = 90^{\circ}$, $\gamma = 120^{\circ}$) with two independent protein molecules per asymmetric unit. Diffraction data up to 2.1 Å resolution were measured at beamline ID29 at the ESRF (Grenoble, France) on a Pilatus 6M detector, and the structure of the esterase has been solved by molecular replacement. At that moment there were two sets of atomic coordinates for Cest-2923 in the Protein Data Bank, one deposited by the Northeast Structural Genomics Consortium (PDB code: 3d3n) and the other one by the Joint Center for Structural Genomics (PDB code: 3bxp). Previous inspection of these models revealed two aspects: first, the two independent molecules of the corresponding asymmetric units were incomplete, lacking a catalytically relevant region around residues Gly231 to Tyr250, and second and most remarkably, they exhibited structural features incompatible with the presence of the catalytic triad typical of an α/β-hydrolase fold, which is the basic architecture of this enzyme. These latter anomalous features will be treated in detail below. Only the shortest deposited model for Cest-2923 (molecule A from the PDB entry 3d3n) is devoid of these anomalous structural features and therefore used as search model. This model lacks the 25-residue sequence stretch between residues Gly231 and Ala255, in conflict with the classic definition of the catalytic triad since it contains the catalytic residue His233 (see below), plus a 3-residue loop (Phe28-Thr30).

In this regard, the residues forming the catalytic triad of Cest-2923 (Ser116, His233 and Asp201) were predicted in a straightforward manner from a simple BLAST search against the PDB, which in turn revealed the putative sugar hydrolase YeeB from *Lactococcus lactis* (PDB entry 3hxk) and the carboxylesterase lp_1002 (PDB entry 3bjr) as the closest homologs (33 and 32% sequence identity, respectively) structurally characterized (**Fig 1**).

The two Cest-2923 independent molecules making up the asymmetric unit of our hexagonal crystal are essentially identical (0.36 Å rmsd for 275 Cα atoms). We arbitrarily chose chain A as reference for description of the protein. As indicated above, the structure of the Cest-2923 subunit is based on a canonical α/β hydrolase fold [6-8] consisting of a central eight-stranded β-sheet, with strand β2 being the only antiparallel strand (**Fig. 2**). The β-sheet shows a marked left-handed twist with an approximate angle of 90º between strands β1 and β8. This core is surrounded by five helices with α1 (Ala54-Met61) and α7 (Trp258-Glu268) lying in one side of the sheet and α2 (Trp84-His103), α3 (Ala117-Val128) and α6 (Ile207-Gln218) on the opposite one. Although Cest-2923 is currently classified as member of the hormone-sensitive lipase subfamily (HSL) of α/β hydrolases [13] by the ESTHER database, the enzyme does not exhibit a distinct cap domain over the active site. Curiously, the loop between strand β8 (Thr223-Phe228) and helix α7 is highly flexible as deduced from the above mentioned models from the JCSG and NESG consortia for the enzyme where this region cannot be modelled, and may perhaps function as a pseudo-flap.

Comparison with other esterases

A DALI search [14] revealed numerous structures with high structural similarity, as otherwise expected due to the high level of conservation of the α/β hydrolase fold [6-8]. Sugar hydrolase YeeB from *Lactococcus lactis* (PDB entry: 3hxk) and carboxylesterase lp_1002 from *Lactobacillus plantarum* WCFS1 (PDB entry: 3bjr) have the highest structural similarity (*Z*-score = 34.7 and 28.8; rmsd = 1.5 and 2.0 Å for 250 and 244 Cα atoms, respectively). Other esterases from the HSL subfamily such as Est1 from environmental samples [15], Sto-Est from *Sulfolobus tokodaii* [16], PestE from *Pyrobaculum calidifontis* [17] and acetyl esterase from *Salmonella typhimurium* (PDB entry: 3ga7) are also structurally similar (*Z*-score = 25.4, 24.8, 24.6 and 24.5; rmsd = 2.5, 2.6, 2.5 and 2.6 Å for 236, 236, 234 and 240 Cα atoms, respectively). In these latter cases, the structural similarity is limited to the α/β hydrolase fold (core β-sheet plus the two surrounding layers of α-helices), since as above indicated Cest-2923 lacks a cap domain characteristic of some HSL enzymes.

Definition of the active site of Cest-2923: the catalytic triad

As a member of the α/β hydrolase superfamily, the catalytic machinery of Cest-2923 is based on a catalytic triad formed by Ser, His, and Asp/Glu residues (Ser116, His233 and Asp201), which are located at canonical sites along the protein sequence. The nucleophile Ser116 of Cest-2923 is situated in the so-called nucleophilic elbow, within a highly conserved sequence (Gly-X-Ser-X-Gly) (with X denoting any amino acid) [13], with its backbone angles residing in an unfavourable region of the Ramachandran plot ($\phi = 52º$, $\psi = -118º$). This constrained conformation is stabilized by a dense network of hydrogen bonds affecting both to the polypeptide chain (two 2.9 Å hydrogen bonds between the carbonyl oxygen atom and the amide nitrogen atoms of Gly119 and Val156, respectively, and a 3.0 Å hydrogen bond between the amide nitrogen atom of Ser116 and the carbonyl oxygen of Gly153), and to the hydroxyl side chain (a hydrogen bond (2.8 Å) between the Oγ atom and the Nε2 atom of His233) (**Fig 3a**).

The proton carrier residues His233 and Asp201 of the charge-relay system locate downstream the strands β8 and β7, respectively. Particularly, the amino acid His233 is located within the 29-residue long loop connecting strand β8 to helix α7. The Nδ1 atom of His233 is hydrogen bonded to the Oδ1 atom (2.7 Å) and to the Oδ2 atom (3.1 Å) of Asp201. The conformation of this last side chain is further stabilized by a hydrogen bond between the Oδ2 atom and the NH of Val204 (2.9 Å) and is also at hydrogen bond distance to the CO of this latter residue (3.1 Å). In addition, the Oδ1 atom is hydrogen bonded to the Nε2 atom of Gln197 (3.0 Å) and also to a highly ordered water molecule (2.7 Å). This solvent molecule together with its close interacting neighbour (2.9 Å distance between them) are present in all structural homologs of Cest-2923 found with DALI and have been proposed to play a structural role in this family of enzymes [18]. In particular, in Cest-2923 these solvent molecules may contribute to maintain the proper conformation of this part of the active site by bridging the loops where His233 and Asp201 are situated. Thus, molecule HOH45 hydrogen bonds to NH atom (3.0 Å) and to the Oγ1 atom (2.8 Å) of Thr198 from the loop connecting strand β7 to helix α6, and HOH4 makes hydrogen bonds to the NH atom (3.1 Å) of Leu235 and to the CO atom (2.8 Å) of Ile232 from the loop between strand β8 and helix α7.

Interestingly, a spherical blob of electron density appeared in close contact to the hydroxyl group of the nucleophile Ser116 of both independent molecules that has been assigned to a sulphate molecule coming from the crystallization solution (**Fig. 3b**). This molecule may be claimed to mimic the negatively charged tetrahedral intermediates of the catalytic reaction, which are stabilized by the so-called oxyanion hole [7]. In this case, the sulphate molecule is stabilized by polar interactions with amide nitrogen atoms of Gly43, Gly44 and Ala117, what would suggest the existence of a tridentate oxyanion hole similar to those from heroin esterase [19], esterase EstE1 [15] or carboxylesterase EST2 from *Alicyclobacillus acidocaldarius* [18], in contrast to the most commonly observed bidentate counterparts [7].

As above indicated, the atomic models of Cest-2923 deposited by the JCSG and NESG consortia (PDB entries 3d3n and 3bxp, respectively), exhibited structural features which are incompatible with the presence of a catalytic triad (**Fig. S1)**. Specifically, in molecule A from PDB entry 3d3n, which is the shortest model, the Asp201 side chain location overlaps with that of His233 (in our model), which in this model is not defined (**Fig. S1a**). Conversely, the trace of the loop that contains the catalytic residue His233 in molecule B places this residue at a distance of 15 Å from the nucleophile Ser116 (distance between Cα atoms), a geometry incompatible with the built-up of a catalytic triad (**Fig. S1b**). Conversely, the conformation of the connecting loop between strand β7 and helix α6 almost coincides with our model, placing the catalytic Asp201 in a similar position. Similar anomalous structural features can be detected in molecules A and B from PDB entry 3bxp (**Fig. S1b**): in this case, the trace of the connecting loop between strand β7 and helix α6 from molecule A places Asp233 in a wrong position and orientation, preventing the catalytic His233 residue to be located in its proper, canonical position, close to the nucleophile Ser116 (**Fig. S1c**). Finally, similar features can be identified in molecule B (**Fig. S1d**).

Oligomeric states of Cest_Lp2923: a case of pH-dependent pleomorphism

The two molecules in the asymmetric unit of the Cest-2923 hexagonal crystal tightly associate, forming a dimer. The association mode is similar to the one observed for other dimeric esterases from the α/β hydrolase superfamily [16, 17] and involves the antiparallel association between β8 strands and interactions between helices preceding (α6) and following (α7) this latter β strand (**Fig. 4a**). We will refer

to these dimers as canonical ones. Analysis of the interfaces within the Cest-2923 crystal with PISA [20] and PIC [21] web servers reveals that the contact region between monomers has an interface area of ~ 980 $Å^2$. The intermolecular contacts identified in this area are 26 H-bonds, 20 hydrophobic and aromatic-aromatic interactions and 2 salt bridges. Among the set of hydrogen bonds detected there are four between main chain atoms, which are those directly involved in the association between β8 strands (particularly, from residues Tyr225 and Leu227).

In addition, this same analysis revealed the existence of a second contact region between symmetry related molecules (molecules A-A and B-B) involving an even larger interface area (1460 $Å^2$). The assembly of Cest_Lp2923 monomers through the joint combination of these two contact regions renders a tetrameric structure made up of two canonical dimers, which is stable according to PISA (total buried area: 9780 $Å^2$; Gibb´s free energy of dissociation, ΔG^{diss}: 11.5 kcal mol^{-1}) (**Fig. 4b**). In this regard, it is worth to note that canonical dimers of close relatives of Cest-2923 such as EstE1 [15], Sto-Est [16], PestE [17], and Brefeldin A esterase [22] also form tetramers within the crystals ("canonical tetramers"), which nevertheless, are not comparable to the one observed for Cest-2923 (**Fig. 4c**). It is obvious that these observations raise the question of whether the Cest-2923 tetramers are crystallographic, i.e. by-product of the crystallization process. In this regard, results from different experimental approaches reveal a complex behaviour of Cest-2923: first, the crystal forms analysed by the structural genomics consortia (PDB entries 3d3n and 3bxp) reveal canonical dimers as the highest order oligomeric form within the crystals, what would support the crystallographic nature of the observed tetramers. In contrast to this, analyses of the oligomeric state of Cest-2923 in solution by analytical ultracentrifugation techniques (**Fig. 5**) reveals a complex scenario, which is consistent with an associative system involving monomeric, dimeric and tetrameric species. Thus, sedimentation velocity studies carried out in Tris buffer (20 mM Tris, pH 8.0, with 0.1 M NaCl) show that Cest-2923 behaves as (at least) two molecular species in solution, with sedimentation coefficients of 3.2 ± 0,2 S (n = 3) and 6.6 ± 0,1 S (n = 3), and estimated average molecular masses of 32 kDa and 96 kDa, respectively, which are values consistent with monomeric and trimeric Cest-2923 species (**Fig. 5a**). Considering the above crystallographic results, where dimers and tetramers have been observed for this protein, this scenario can be easily explained in terms of two association equilibria: a fast equilibrium (within the time scale of the sedimentation velocity

experiment, namely 6 hours) between dimers and tetramers, therefore explaining the average molecular mass of the 6.8 S species (intermediate between dimers and tetramers), and a second, slow equilibrium between monomers and dimers, therefore explaining the peak assignable to the monomer.

As expected from these latter ultracentrifugation results, sedimentation equilibrium experiments carried out under identical experimental conditions, fitted well to a monomer to tetramer association scheme, but also to an ideal model considering a unique species with an estimated average molecular mass of 69.8 ± 5.4 kDa (**Figs. 5b and 5c**) what would indicate that the system is mainly shifted to the dimeric species under neutral conditions. In this regard, it is worth to note that the two crystal forms prepared by the structural genomics consortia, where only canonical dimers were observed, were both obtained at pH 7.5 (PDB entry 3bxp: 30% 1,2-propanediol, 20% PEG 400, 0.1 M HEPES, pH 7.5; PDB entry 3d3n: 5% PEG 8000, 0.1 M calcium acetate, 0.1 M HEPES, pH 7.5).

Conversely, since the Cest-2923 crystals described in this work, which revealed the presence of tetramers, were obtained in 1.7 M ammonium sulphate, 0.15 M sodium acetate, pH 4.6, we also analysed the behaviour of the enzyme in solution at acidic conditions. Unexpectedly, we found that Cest-2923 precipitates in sodium acetate buffer (20 mM sodium acetate, pH 4.6 with 0.1 M NaCl) even at low protein concentration (0.2 mg/ml), but it was stable at pH 5.5. In this regard, both the far-UV CD spectrum at 25 ºC and the thermal denaturation curve measured in acetate buffer, pH 5.5 are indistinguishable from those registered at pH 8.0, indicating that there are no significant structural differences and changes in stability **(Fig. S2)**. Under these acidic conditions, sedimentation velocity analyses revealed a similar profile as those observed at pH 8.0, although with a relative lower contribution of the monomeric species for samples with the same protein concentration in comparable experiments (not shown). As expected, sedimentation equilibrium experiments fitted well to a monomer to tetramer associative model, and also to an ideal one with a unique species with an average molecular mass of 98.6 ± 0,6 kDa (**Figs. 5d and 5e**), indicating a displacement of the equilibria towards the tetrameric form relative to the neutral conditions.

Combining the results derived from these two distinct experimental approaches (crystallographic and analytical ultracentrifugation) we can deduce that Cest-2923 behaves in solution as an associative system well described by two equilibria, namely, a fast equilibrium between species with molecular

masses consistent with monomers and dimers and another, much faster one between dimeric and tetrameric species, and secondly that the crystallization process is an active player in selecting a pre-existing oligomeric form: dimers at neutral conditions, tetramers at acidic ones. Hence, we claim that the oligomeric forms determined by protein crystallography are not a mere crystallographic by-product but reveal intrinsic, associative properties of Cest-2923. Nevertheless, determination of the structural basis of the pH-dependence of the complex associative behaviour of Cest-2923 is not straightforward. Analysis of the interactions between Cest-2923 subunits with PISA [20] and PIC [21] revealed that the hydrophobic and H-bond interactions are the main driving force for protein association, mainly for dimer formation but also for tetramer formation. If this is the case, a displacement of the association equilibria towards tetramer formation can be predicted both under acidic or basic conditions with respect to the Cest-2923 isoelectric point (theoretical value: 6.5). In this sense, we carried out analytical ultracentrifugation studies of Cest-2923 at pH 9.0 (20 mM Tris, pH 9.0, 0.1 M NaCl) essentially as above (both sedimentation velocity and equilibrium assays). The obtained results (**Fig. S3**) are similar to those obtained under acidic conditions in agreement with an association process mainly guided by hydrophobic interactions.

As indicated above, EstE1 [15], Sto-Est [16], PestE [17], and Brefeldin A esterase [22] form canonical tetramers within the crystals (**Fig. 4c**). These tetramers have not been considered a crystallographic by-product since they were observed in different crystal lattices with crystals prepared in disparate conditions. It is worth to remark that this conclusion was derived despite these proteins were dimers in solution at much lower concentrations [17]. It is obvious that this behaviour resembles the one described here for Cest-2923 and therefore similar association equilibria for these proteins cannot be dismissed. From a structural viewpoint, Cest-2923 tetramers are not canonical ones, and are almost perfectly superimposable to those of the putative sugar hydrolase YeeB from *Lactococcus lactis* (PDB entry 3hxk), one of its closest structural relatives (**Fig. 4d**). When compared, it can be seen that both canonical and non canonical tetramers result from a head-to-head association since the same region from both canonical dimers is the one involved in association, although this region is different in both types of tetramers: thus, defining the *cis* face of the dimers as the one in which the C-terminal α-helix of the participating monomers is situated, non canonical tetramers would result from a *cis*-to-*cis* association whereas canonical ones would result from a *trans*-to-*trans* association. In both cases the final oligomer

exhibits a 222 point group although it is evident that the relative orientation of the dimers within tetramers is also different: if one dimer of each tetramer is fixed as a reference and is equally oriented for comparison the other dimers are rotated with respect to each other around 60º (**Fig. S4**).

As a whole, these results indicate that Cest-2923 displays a pleomorphic behaviour since it can form different oligomeric assemblies depending on pH, protein concentration and probably other environmental conditions as can be derived from crystallization experiments. We believe that this behaviour reflects an intrinsic property of the enzyme although on the other hand, we have no experimental basis to claim that this property has functional consequences *in vivo*. Undoubtedly, this needs to be further investigated.

Biochemical characterization

The most relevant enzymatic properties of Cest-2923 have been examined (**Fig. 6**). The optimum pH for hydrolytic activity against *p*-nitrophenyl acetate (see below) is 7.0 (**Fig. 6a**), which is a value typically observed for esterases, in contrast to the higher pH values (~ 8.0) displayed by lipases [23]. Regarding to temperature, the esterase presented highest activity at ~30 ºC, although at 45 ºC it exhibited a high level of activity (~65%) (**Fig. 6b**). These values for optimum pH and temperature are commonly found in other esterases from Lactobacilli [24-26]. On the other hand, temperature stability measurements show a drastic reduction in Cest-2923 hydrolytic activity upon incubation of the esterase at 55 ºC (**Fig. 6c**). This result agrees well with the analysis of protein thermostability carried out by far-UV CD spectroscopy, which revealed an apparent $T_{1/2}$ value around 60 ºC at neutral and acidic pH values **(Fig. S2)**.

The acyl-length selectivity against *p*-nitrophenyl ester substrates follows this order: C2 > C4 > C8 > C12 > C14, indicating a preference for short acyl-length esters (**Fig. 6d**). The kinetic parameters for C2 and C4 substrates were determined spectrophotometrically. In both cases, Cest-2923 exhibited a hyperbolic Michaelis-Menten kinetics (not shown). The kinetic parameters are shown in **Table 2**. From the values of these parameters it can be deduced that the catalytic efficiency (k_{cat}/K_m) for pNPA hydrolysis is around 75-fold the one observed for pNPB hydrolysis. Also, substrate specificity has been analysed with the use of a library of esters as described previously [27]. This study reveals maximum hydrolysis against phenyl acetate, which is considered as reference (100% activity), and also significant

activity (> 10% of the activity observed for phenyl acetate) against methyl bromoacetate and isopropenyl acetate. Within the limitations of the ester library employed, this result suggests a broader specificity for the alcohol part of the substrate and preference for small moieties for the acid part.

These three substrates were subsequently used for crystallographic studies with the aim to determine the structure of the corresponding complexes. With this purpose, native crystals were incubated for ~60 secs with a cryosolution containing the substrate at a concentration of 10 mM. Diffraction data recorded at beamline ID23-1 from the ESRF (Grenoble, France) with two types of these crystals (those prepared with methyl bromoacetate rapidly cracked) permitted to solve their structure, which unfortunately did not result in the structure of the complexes but unexpectedly provided evidences of catalysis occurring within the crystals. Thus, we observed that upon incubation with the corresponding cryosolution the space group of the native crystals ($P6_322$) changed: those crystals incubated with phenyl acetate became monoclinic (*C*2 space group) whereas those incubated with isopropenyl acetate changed to the *P*622 hexagonal space group. Interestingly, in both cases, the hexagonal packing was preserved and, in fact, indexing of the diffraction data identified the native unit cell and 622 point group what suggests that these changes in crystal symmetry result from the ordered incorporation of new molecules within the crystal lattice (see **Table 1**). One interesting observation is the presence in both types of crystals of an acetate molecule in the vicinity of the nucleophile Ser116, instead of a sulphate molecule which appeared in native crystals (**Fig. S5**). We believe this is remarkable since acetate by itself cannot replace sulphate in the active site as deduced from the native structure. We interpret this result as the substitution of sulphate by the corresponding substrate, which is further hydrolysed. After this step, the alcohol is released in contrast to the acetate molecule, which remains in the active site.

Materials and methods

Bacterial strains, plasmids and DNA manipulations

L. plantarum WCFS1 was grown in MRS medium at 30ºC without shaking [28]. *Escherichia coli* DH10B was used for all DNA manipulations and *E. coli* BL21 (DE3) was used for expression in pURI3-Cter vector [29]. *E. coli* strains were cultured in Luria-Bertani (LB) medium at 37ºC and 140 rpm.

The gene *lp_2923* from *L. plantarum* WCFS1 coding for Cest-2923 was cloned and overexpressed following a strategy previously described [30]. Briefly, the gene was PCR-amplified with HS Prime Start DNA polymerase (Takara) by using the primers 856 (TAACTTTAAGAAGGAGA TATACATatgcaagttgaacagcgcaca) and 857 (GCTATTAATGATGATGATGATGATGataattacc agctaacaatc) (the nucleotides pairing the expression vector sequence are indicated in uppercase characters, and the nucleotides pairing the *lp_2923* gene sequence are written in lowercase characters). The corresponding 831pb purified PCR product was inserted into the pURI3-Cter vector by using the restriction enzyme- and ligation-free cloning procedure to produce C-terminally His-tagged Cest-2923 essentially as described previously [30].

E. coli DH10B cells were transformed, recombinant plasmids were isolated, and those containing the correct insert were identified by restriction-enzyme analysis, verified by DNA sequencing, and then transformed into *E. coli* BL21 (DE3) cells.

Expression and purification of recombinant Cest-2923

Cells carrying the recombinant plasmid pURI3-Cter-lp_2923 were grown at 37 ºC in LB media containing ampicillin (100 µg/ml) and induced by adding 0.4 mM isopropyl-β-D-thiogalactopyranoside. After induction, the cells were grown at 22 ºC during 20 h and collected by centrifugation using a Beckman Coulter J-25 Avanti centrifuge (7500 x g for 15 min at 4 ºC). Cells were resuspended in 20 ml of 20 mM Tris-HCl, pH 8.0 containing 100 mM NaCl per liter of cell culture. Crude extracts were prepared by French Press lysis of cell suspensions. The lysate was centrifuged at 17,400 x g for 40 min at 4 ºC using a Beckman Coulter J-25 Avanti centrifuge.

The supernatant was filtered through a 0.22 µm filter (Millipore) and subsequently loaded onto a HisTrap-FF column previously equilibrated in binding buffer (20 mM Tris-HCl, pH 8.0 containing 100

mM NaCl and 10 mM imidazole). The recombinant His-tagged Cest-2923 was eluted with a linear gradient of imidazole (from 10 mM to 500 mM) with an ÄKTA Prime Plus. Fractions containing Cest-2923 were pooled and concentrated by ultrafiltration with a YM-10 membrane (Amicon). The protein (2 ml) was then loaded onto a HiLoad™ 16/60 Superdex 200 prep-grade (GE Healthcare) equilibrated in Tris buffer (20 mM Tris-HCl, pH 8.0 containing 100 mM NaCl). The purity of the enzyme was checked by SDS-PAGE. Pure protein was finally concentrated to 10 mg/ml for crystallization trials by ultrafiltration and stored at -80 ºC until use.

Enzyme activity assay

Esterase activity was determined spectrophotometrically using *p*-nitrophenyl acetate as substrate. The rate of hydrolysis of *p*-NP acetate for 10 min at 30 ºC was measured in 50 mM sodium phosphate buffer pH 7.0 at 348 nm in a spectrophotometer (UVmini-1240 Shimadzu). The reaction was stopped by chilling on ice.

In order to carry out the reaction a stock solution of 25 mM of *p*-NP acetate was prepared in acetonitrile/isopropanol (1/4 *v/v*) [31] and mixed with 50 mM sodium phosphate buffer, pH 7.0 to obtain a substrate final concentration of 1 mM. Reaction was initiated by adding 10 µg of protein. Control reactions containing no enzyme were utilized to account for any spontaneous hydrolysis of the substrates tested. Enzyme assays were performed in triplicate. One unit of esterase activity was defined as the amount of enzyme required to release 1 µmol of *p*-nitrophenol per minute under the previously described conditions.

Substrate specificity

The substrate specificity of Cest-2923 was investigated with two different approaches: first, we studied the dependence of the hydrolytic activity of the enzyme on the aliphatic chain length of the substrates by using *p*-nitrophenyl (*p*-NP) esters with various chain lengths: *p*-NP acetate (C2); *p*-NP butyrate (C4); *p*-NP caprylate (C8); *p*-NP laurate (C12) and *p*-NP myristate (C14) essentially as described previously [10]. Briefly, a stock solution of each *p*-NP ester was prepared in acetonitrile/isopropanol (1/4 *v/v*). Substrates were emulsified to a final concentration of 0.5 mM in 50 mM sodium phosphate buffer, pH 7.0,

containing 1.1 mg/ml Arabic gum and 4.4 mg/ml Triton X-100. The reaction mix consisted of 990 µl of emulsified substrate and 10 µl of enzyme solution (10 µg of protein). Reactions were carried out at 30 ºC in a spectrophotometer (UVmini-1240 Shimadzu) as described above.

Second, substrate specificity was also analysed using the ester library described previously by Liu et al [9]. Briefly, the screening was performed in a 96-well plate Flat Bottom (Sarstedt) where final reaction volume was 200 µl and each well contained a different substrate (1 mM final concentration in 1 % acetonitrile). A buffer/indicator solution containing 0.44 mM of *p*-nitrophenol was used as pH indicator in 1 mM sodium phosphate buffer pH 7.2. Cest-2923 (10 µg in 20 µl of 1 mM sodium phosphate buffer pH 7.2) was added to each well and reactions were followed by measuring the decrease in absorbance at 410 nm for 2 h at 30ºC in a Synergy HT BioTek microplate spectrophotometer. Blanks without enzyme were carried out for each substrate and data were collected in triplicate.

The general ester library consisted of 50 commercially available esters. These were chosen to identify not only acyl chain length preferences of the hydrolases but also their ability to hydrolyse hindered or charged substrates. Simple alkyl esters as well as activated esters (vinyl and phenyl esters, esters with electron-withdrawing substituents in the acyl portion) were included to test whether activated esters would react faster.

Biochemical characterization of Cest-2923

In order to investigate temperature effect, reactions were performed in 50 mM sodium phosphate buffer (pH 7.0) at 4, 20, 30, 37, 40, 45, 55 and 65 ºC. Effect of pH was investigated by assaying esterase activity in a range of pH values from 5.5 to 9.0 at 30 ºC. Buffers used were acetic acid-sodium acetate buffer for pH 5.5, sodium phosphate buffer for pH 6-7, Tris-HCl buffer for pH 8 and glycine-NaOH buffer for pH 9. A 100 mM concentration was used in all the buffers. Although initially activity measurements were done at lower pH values (between 3.0 and 5.0) these are not reported since protein aggregation was detected in acetate buffer pH 4.6 or 5.0.

For temperature stability measurements, the recombinant esterase was incubated in 50 mM sodium phosphate buffer pH 7.0 at 20, 30, 37, 45, 55 and 65 ºC for 15 min, 30 min, and 1, 2, 3, 4, 6 and 20 h. After incubation, the residual activity was measured as described above.

Analytical ultracentrifugation

Equilibrium and sedimentation velocity ultracentrifugation experiments were performed at 10,500 rpm, 20ºC, using a Beckman XL-A ultracentrifuge with an An-50Ti rotor and standard double sector centerpiece cells. Solvent density (1.0029 mg/ml) and the partial specific volume of Cest-2923 (0.719) were calculated from the buffer composition (100 mM NaCl, 20 mM Tris-HCl or 100 mM NaCl, 20 mM sodium acetate) and from the predicted amino acid composition, respectively, with SEDNTERP [32]. Data from sedimentation velocity and equilibrium experiments were analysed using the programs Sedfit [33] and Heteroanalysis [34], respectively.

Circular dichroism spectroscopy

Far-UV circular dichroism (CD) measurements were carried out on a Jasco J-715 spectropolarimeter equipped with a thermostated cell holder and a Peltier temperature control accessory. The instrument was calibrated with (+)-10-camphorsulfonic acid. CD spectra were recorded in 0.1 cm path length quartz cell cuvettes from 250 to 205 nm, using a protein concentration of 6.4 μM (1 nm bandwidth, 4 s response, and 20 nm/min scan speed). Each spectrum herein presented is the average accumulation of four scans. Baseline subtraction was performed in all cases. Results are expressed as mean residue ellipticity $[\theta]_{MRW}$, in units of degree cm^2 $dmol^{-1}$ of amino acid (Mr = 110 for this protein). Thermal transitions were also analysed by CD spectroscopy by monitoring the variation of the ellipticity at 218 nm as the temperature was increased from 20 to 90 ºC at 50 ºC/h. The normalized ellipticity value at each temperature was calculated as $([\theta]_T-[\theta]_{25})/([\theta]_{90}-[\theta]_{25})$, where $[\theta]_T$ is the ellipticity value at temperature T, and $[\theta]_{25}$ and $[\theta]_{90}$ are the ellipticity values at 25 ºC and 90 ºC, respectively. Three different samples were analysed, although the traces shown correspond to individual samples.

Crystallization and data collection

Initial crystallization conditions for Cest-2923 were determined by the sitting-drop vapour diffusion method with commercial screens from Hampton Research (Riverside, California, USA) in Innovaplate

SD-2 96-well plates set up using a Nanodrop Innovadyne robot. Each drop contained 250 nl of protein (7 mg/ml) in Tris–HCl buffer (20 mM Tris–HCl pH 8.0 containing 0.1 M NaCl) and 250 nl of reservoir solution. Drops were equilibrated against 65 µl reservoir solution. Scaling up of the crystallization conditions using hanging drops in 24-well VDX plates (2:1 protein:precipitant volume ratio; total volume 3 µl) rendered high quality diffracting crystals in 1.7 M ammonium sulphate, 0.15 M sodium acetate, pH 4.6. Crystals suitable for X-ray analysis were transferred to an optimized cryoprotectant solution (reservoir solution plus 20% (*v/v*) 2-methyl-2,4-pentanediol) for ~10 secs and then cryocooled at 100 K in the cold nitrogen-gas stream. Diffraction data were recorded on a Pilatus 6M detector (Area Detector Systems Corp.) at beamline ID29 at the European Synchrotron Radiation Facility (ESRF) (Grenoble, France). Diffraction images were processed with XDS [35] and the data scaled and analysed using SCALA [36] from the CCP4 software suite [37]. Cryosoaking experiments were carried out with native Cest-2923 crystals, with a cryosolution containing phenyl acetate or isopropenyl acetate (10 mM final concentration. These new crystals were measured at beamline ID23-1 at the ESRF. Diffraction data were recorded on a Pilatus 6M-F detector (Area Detector Systems Corp.). Data statistics are summarized in **Table 1**.

Structure determination and refinement

The crystal structure of Cest-2923 was determined by the molecular replacement method with PHASER [38] using the PHENIX software suite [39]. The atomic coordinates of the enzyme deposited by the Northeast Structural Genomics Consortium (PDB code: 3d3n) were used as search model. Importantly, the 25-residue long loop containing the catalytic His233 residue not defined in this model could be modeled with the diffraction data obtained from the new crystal form described in this work. Conversely, the atomic model deposited by the Joint Center for Structural Genomics for Cest_Lest-2923 (PDB code: 3bxp) is discussed above. Restraint refinement and automatic water molecule placement was done with phenix-refine [40]. Stereochemical validation was carried out using the program MOLPROBITY [41]. The refinement statistics are summarized in **Table 1**. The final model has an R-factor of 15.5 % and an R_{free} of 19.5 %, and included 550 amino acid residues, 9 sulphate molecules, 3 acetate molecules, 1 Tris and 520 solvent molecules. Details on the structures derived from crystals soaked with substrates phenyl

acetate and isopropenyl acetate can be seen in **Table 1**. The PISA [20] and PIC [21] webservers were used to calculate values of buried interface areas. Ribbon diagrams were prepared using PyMOL [42].

Acknowledgements

We thank the ESRF (Grenoble, France) for provision of synchrotron radiation facilities (ID29 and ID23-1). JMM thanks Margarita Menéndez for her helpful advices on ultracentrifugation analyses. Financial support from the Ministerio de Economía y Competitividad (BFU2010-17929/BMC) and the Factoría de Cristalización (Consolider-Ingenio-2007) (to J.M.M.), AGL2011-22745 (to R. M.), FUN-C-FOOD Consolider 25506 (to R. M.) is greatly appreciated. Y.A., M.E-T. and I.A. and are recipients of the following fellowships: CSIC-CITMA, JAE Predoc (CSIC), FPU (MEC), respectively.

References

1. Bornscheuer UT (2002) Microbial carboxyl esterases: classification, properties and application in biocatalysis. *FEMS Microbiol Rev* **26**, 73-81.

2. Jaeger KE, Dijkstra BW & Reetz MT (1999) Bacterial biocatalysts: molecular biology, three-dimensional structures, and biotechnological applications of lipases. *Annu Rev Microbiol* **53**, 315-351.

3. Arpigny JL & Jaeger KE (1999) Bacterial lipolytic enzymes: classification and properties. *Biochem J* **343**, 177-183.

4. Hotelier T, Renault L, Cousin X, Negre V, Matchot P & Chatonnet A (2004) ESTHER, the database of the alpha/beta hydrolase fold superfamily of proteins. *Nucleic Acids Res* **32**: D145.

5. Holm C, Osterlund T, Laurell H & Contreras JA (2000) Molecular mechanisms regulating hormone-sensitive lipase and lipolysis. *Annu Rev Nutr* **20**, 365-393.

6. Ollis DL, Cheah E, Cygler M, Dijkstra B, Frolow F, Franken SM, Harel M, Remington SJ, Silman I, Schrag J, et al. (1992) The alpha/beta hydrolase fold. *Protein Eng* **5**, 197-211.

7. Nardini M & Dijkstra BW (1999) α/β hydrolase fold enzymes: the family keeps growing. *Curr Opin Struct Biol* **9**, 732-737.

8. Heikinheimo P, Goldman A, Jeffries C & Ollis DL (1999) Of barn owls and bankers: a lush variety of α/β hydrolases. *Structure* **7**, R141-R146.

9. Rodríguez H, Curiel JA, Landete JM, de las Rivas B, López de Felipe F, Gómez-Cordovés C, Mancheño JM & Muñoz R (2009) Food phenolics and lactic acid bacteria. *Int J Food Microbiol* **132**, 79-90.

10. Brod FCA, Vernal J, Bertoldo JB, Terenzi H & Arisi ACM (2010) Cloning, expression, purification, and characterization of a novel esterase from *Lactobacillus plantarum*. *Mol Biotechnol* **44**, 242-249.

11. Kleerebezem M, Boekhorst J, Kranenburg R, Molenaar D, Kuipers OP, Leer R, Tarchini R, Peters SA, Sandbrink HM, Fiers MWEJ, Stiekema W, Lankhorst RMK, Bron PA, Hoffer SM, Groot MNN, Kerkhoven R, de Vries M, Ursing B, de Vos WM & Siezen RJ (2003) Complete genome sequence of *Lactobacillus plantarum* WCFS1. *Proc Natl Acad Sci USA* **100**, 1990-1995.

12. Álvarez Y, Esteban-Torres M, Acebrón I, de las Rivas B, Muñoz R, Martínez-Ripoll M & Mancheño JM (2011) Preliminary X-ray analysis of twinned crystals of the Q88Y25_Lacpl esterase from *Lactobacillus plantarum. Acta Crystallog* F**67**, 1436-1439.

13. Hemilä H, Koivula TT & Palva I (1994) Hormone-sensitive lipase is closely related to several bacterial proteins, and distantly related to acetylcholinesterase and lipoprotein lipase: identification of a superfamily of esterases and lipases. *Biochim Biophys Acta* **1210**, 249-253.

14. Holm L & Rosenström P (2010) Dali server: conservation mapping in 3D. *Nucleic Acids Res* **38**, W545-W549.

15. Byun JS, Rhee JK, Kim ND, Yoon JH, Kim DU, Koh E, Oh JW & Cho HS (2007) Crystal structure of hyperthermophilic esterase Est1 and the relationship between its dimerization and thermostability properties. *BMC Struct Biol* **7**, 47-57.

16. Angkawidjaja C, Koga Y, Takano K & Kanaya S (2012) Structure and stability of a thermostable carboxylesterase from the thermoacidiphilic archaeon *Sulfolobus tokodaii*. *FEBS J* **279**, 3071-3084.

17. Palm GJ, Fernández-Álvaro E, Bogdanović X, Bartsch S, Sczodrok J, Singh RK, Böttchner D, Atomi H, Bornscheuer UT & Hinrichs W (2011) The crystal structure of an esterase from the hyperthermophilic microorganism *Pyrobaculum calidifontis* VA1 explains its enantioselectivity. *Appl Microbiol Biotechnol* **91**, 1061-1072.

18. De Simone G, Galdiero S, Manco G, Lang D, Rossi M & Pedone C (2000) A snapshot of a transition state analogue of a novel thermophilic esterase belonging to the family of mammalian hormone-sensitive lipase. *J Mol Biol* **303**, 761-771.

19. Zhu X, Larsen NA, Basran A, Bruce NC & Wilson IA (2003) Observation of an arsenic adduct in an acetyl esterase crystal structure. *J Biol Chem* **278**, 2008-2014.

20. Krissinel E & Henrick K (2007) Inference of macromolecular assemblies from crystalline state. *J Mol Biol* **372**, 774-797.

21. Tina KG, Bhadra R & Srinivasan N (2007) PIC, Protein Interactions Calculator. *Nucleic Acids Res* **35**, W473-W476.

22. Wei Y, Contreras JA, Sheffield P, Osterlund T, Derewenda U, Kneusel RE, Matern U, Holm C & Derewenda ZS (1999) Crystal structure of brefeldin A esterase, a bacterial homolog of the mammalian hormone-sensitive lipase. *Nature Struc Biol* **6**, 340-345.

23. Fojan P, Jonson PH, Petersen MTN & Petersen SB (2000) What distinguishes an esterase from a lipase: A novel structural approach. *Biochimie* **82**, 1033-1041.

24. Gobbeti M, Fox PF, Smacchi E, Stepaniak L & Damiani P (1996) Purification and characterization of a lipase from *Lactobacillus plantarum* 2739. *J Food Biochem* **20**, 227-246.

25. Fenster KM, Perkin KL & Steele JL (2003) Intracellular esterase from *Lactobacillus casei* LILA: nucleotide sequencing, purification and characterization. *J Dairy Sci* **86**, 1118-1129.

26. Gobbeti M, Fox PF, Smacchi E & Stepaniak L (1997) Isolation and characterization of a tributyrin esterase from *Lactobacillus plantarum* 2739. *J Dairy Sci* **80**, 3099-3106.

27. Liu AMF, Somers NA, Kazlauskas RJ, Brush TS, Zocher TS, Enzelberger MM, Bornscheuer UT, Horsman GP, Mezzetti A, Schmidt-Dannert C & Schmid RD (2001) Mapping the substrate selectivity of new hydrolases using colorimetric screening: lipases from *Bacillus thermocatenolatus* and *Ophiostoma piliferum*, esterases from *Pseudomonas fluorescens* and *Streptomyces diastatochromogenes*. *Tetrahedron Asym* **12**, 545-556.

28. De Man JC, Rogosa M & Sharpe ME (1960) A medium for the cultivation of lactobacilli. *J Appl Bacteriol* **23,** 130–135.

29. Curiel JA, de las Rivas B, Mancheño JM & Muñoz R (2011) The pURI family of expression vectors: A versatile set of ligation independent cloning plasmids for producing recombinant His-fusion proteins. *Prot Express Purif* **76**, 44–53.

30. De las Rivas B, Curiel JA, Mancheño JM & Muñoz, R (2007) Expression vectors for enzyme restriction- and ligation-independent cloning for producing recombinant His-fusion proteins *Biotechnol. Prog* **23**, 680–686.

31. Glogauer A, Martini VP, Faoro H, Couto GH, Müller-Santos M, Monteiro RA, Mitchel DA, de Souza EM, O Pedrosa F & Krieger N (2011) Identification and characterization of a new true lipase isolated through metagenomic approach. *Microbial Cell Factories* **10**, 54.

32. Laue TM, Shah BD, Ridgeway TM & Pelletier SL (1992) *Biochemistry and Polymer Science.* Royal Society of Chemistry, London.

33. Schuck P (2000) Size distribution analysis of macromolecules by sedimentation velocity ultracentrifugation and Lamm equation modeling. *Biophys J* **78**, 1606-1619.

34. Cole JL & Lary JW (2009) *HeteroAnalysis*. Bioservices Center. University of Connecticut, Storrs, CT, Analytical Ultracentrifugation Facility.

35. Kabsch W (2010) XDS. *Acta Crystallog D Biol Crystallog* **66**, 125-132.

36. Evans PR (2011) An introduction to data reduction: space-group determination, scaling and intensity statistics. *Acta Crystallog D Biol Crystallog* **67**, 282-292.

37. Winn MD, Ballard CC, Cowtan KD, Dodson KD, Emsley P, Evans PR, Keegan RM, Krissinel EB, Leslie AGW, McCoy A, McNicholas SJ, Murshudov GN, Pannu NS, Potterton EA, Powell HR, Read RJ, Vagin A & Wilson KS (2011) Overview of the CCP4 suite and current developments. *Acta Crystallog D Biol Crystallog* **67**, 235-242.

38. McCoy AJ, Grosse-Kunstleve RW, Adams PD, Winn MD, Storoni LC & Read RJ (2007) Phaser crystallographic software. *J Appl Cryst* **40**, 658-674.

39. Adams PD, Afonine PV, Bunkóczi G, Chen VB, Davis IW, Echols N, Headd JJ, Hung LW, Kapral GJ, Grosse-Kunstleve RW, McCoy AJ, Moriarty NW, Oeffner R, Read RJ, Richardson DC, Richardson JS, Terwilliger TC & Zwart PH (2010) PHENIX: a comprehensive Python-based system for macromolecular structure solution. *Acta Crystallog D Biol Crystallog* **66**, 213-221.

40. Afonine PV, Grosse-Kunstleve RW, Echols N, Headd JJ, Moriarty NW, Mustyakimov M, Terwilliger TC, Urzhumtsev A, Zwart PH & Adams PD. (2012) Towards automated crystallographic structure refinement with phenix.refine. *Acta Crystallogr D Biol Crystallogr* **68**, 352-367

41. Chen VB, Arendall III WB, Headd JJ, Keedy DA, Immormino RM, Kapral GJ, Murray LW, Richardson JS & Richardson DC (2010) MolProbity: all-atom structure validation for macromolecular crystallography. *Acta Crystallogr D Biol Crystallogr* **66**, 12-21.

42. DeLano WL (2008) *The PyMOL Molecular Graphics System* (http://www.pymol.org).

Supporting information

Titles of figures

Figure S1. Three dimensional superposition of Cest-2923 from this work with models deposited by structural genomics consortia (3d3n from NSGC; 3bxp from JCSG).

Figure S2. Far-UV CD analysis of Cest-2923 at neutral and acidic conditions.

Figure S3. Analytical ultracentrifugation studies of Cest-2923 at basic conditions indicate a predominance of tetramers over dimers, similarly to acidic conditions.

Figure S4. Three dimensional comparison of non-canonical tetramers of Cest-2923 and canonical tetramers of enzymes from the HSL family.

Figure S5. The presence of acetate molecules in the close vicinity of the nucleophile Ser116 in Cest-2923 crystals soaked with substrates reveal catalysis within the crystal.

Figure legends

Fig. 1. Amino acid sequence alignment of Cest-2923 with its closest homologs. Cest-2923 shares 33% and 32% sequence identity with the putative sugar hydrolase YeeB from *Lactococcus lactis* and the carboxylesterase lp_1002 from *Lactobacillus plantarum*, respectively. Colour code indicates: *blue*, conserved amino acid residues; *yellow*, similar residues; *red*, residues forming the catalytic triad in YeeB and lp_1002.

Fig. 2. Overall fold of the Cest-2923 subunit from *Lactobacillus plantarum* WCFS1. The tertiary structure of the Cest-2923 subunit fits the canonical α/β hydrolase fold where a central eight-stranded β-sheet (shown in *green*) is surrounded by five α-helices (*orange*). Two orthogonal views of the protein subunit are shown.

Fig. 3. Catalytic triad machinery of the Cest-2923 subunit from *Lactobacillus plantarum* WCFS1. (A) Stereo view of the catalytic triad environment of Cest-2923. Residues of the catalytic triad (Ser116, His233, Asp201) are shown as *orange sticks* and those participating in hydrogen bonding interactions as *grey sticks*; potential H-bonds are indicated as *black*, *broken* lines. A conserved water molecule that interacts with Asp201, which is conserved within the HSL family of enzymes, is shown as a *blue* sphere. (B) Stereo view of the surroundings of the sulphate molecule found in the active site of Cest-2923. The electron density map ($2F_o$-F_c in *blue*; contoured at 1-σ level) for the sulphate is shown. Residues of the catalytic triad are shown as *light yellow sticks.* Distances are given in Å.

Fig. 4. Dimeric and tetrameric assemblies of Cest-2923 from *Lactobacillus plantarum* WCFS1. (A) Canonical dimer of Cest-2923. The association of the subunits involves interactions between strands β8 and α-helices α6 and α7. The two subunits are shown in different colours. (B) Non-canonical tetramer of Cest-2923. The contacting region between canonical dimers is mainly formed by α-helix α1, the contacting loops between strands β2 and β3 and between strand β8 and α-helix α7 and the C-terminal

end. The four subunits are shown in different colours. (C) Canonical tetramer of HSL esterases. As an example it is shown the tetramer of the hyperthermophilic esterase EstE1 (PDB entry: 2c7b) [15]. Further details on the comparison between canonical and non-canonical tetramers can be found in Fig. S3. (D) Three dimensional superposition between the non-canonical tetramers of Cest-2923 (in transparent, *grey* cartoons) and those found for the putative sugar hydrolase YeeB from *Lactococcus lactis* (PDB entry 3hxk).

Fig. 5. Analytical ultracentrifugation analysis of Cest-2923 at neutral and acidic conditions. (A) Sedimentation coefficient *c*(*s*) distributions for Cest-2923 (13 μM) in Tris buffer (20 mM Tris-HCl, pH 8.0 with 0.1 M NaCl). Raw sedimentation velocity profiles for this analysis were acquired using absorbance at 280 nm, 45,000 rpm, 20 ºC, and different times (not shown). Calculations were done with the program SEDFIT [33]. (B) Sedimentation equilibrium analysis of Cest-2923 (13 μM) in Tris buffer (20 mM Tris-HCl, pH 8.0 with 0.1 M NaCl) at 12,000 rpm (*open* circles) and 17,300 (*open* squares). Absorbance at 280 nm is plotted against the radial position from the centre of the rotor. The fit to the data set (*solid line curves*) corresponds to a monomer-tetramer association equilibrium. Residuals from this fit are shown in the inset. (C) As the previous panel, but the fit corresponds to an ideal species. The best-fit weight average molecular mass is 69.8 ± 5.4 kDa. (D) Sedimentation equilibrium analysis of Cest-2923 (13 μM) in acetate buffer (20 sodium acetate, pH 5.5 with 0.1 M NaCl) at 13,400 rpm (*open* circles) and 19,500 (*open* squares). Other experimental conditions are identical to those at neutral conditions. The fit to the data set (*solid line curves*) corresponds to a monomer-tetramer association equilibrium. Residuals from this fit are shown in the inset. (E) As panel (D), but the fit corresponds to an ideal species. The best-fit weight average molecular mass is 98.6 ± 0,6 kDa.

Fig. 6. Biochemical characterization of Cest-2923 from *Lactobacillus plantarum* WCFS1. (A) Dependence on pH of hydrolytic activity of Cest-2923 against *p*-nitrophenyl acetate. *Open squares* indicate measurements in Tris buffer (pH 7.0) and phosphate buffer (pH 8.0) carried out to discard buffer-specific side effects. (B) Dependence on temperature of hydrolytic activity of Cest-2923 against *p*-

nitrophenyl acetate. The optimum temperature for esterase activity was ~30 ºC. (C) Analysis of the temperature stability of Cest-2923. Recombinant esterase was incubated in 50 mM sodium phosphate buffer pH 7.0 at 20 (*open circles*), 30 (*closed circles*), 37 (*open squares*), 45 (*closed squares*), 55 (*open triangles*) and 65 ºC (*closed triangles*) for 15 min, 30 min, and 1, 2, 3, 4, 6 and 20 h. In all cases, the values shown are the mean average of three independent experiments. (D) Dependence of the esterase activity of Cest-2923 on the aliphatic chain length of *p*-nitrophenyl (*p*-**NP**): *p*-**NP** acetate (C2); *p*-**NP** butyrate (C4); *p*-**NP** caprylate (C8); *p*-**NP** laurate (C12) and *p*-**NP** myristate (C14).

Table 1. Data Collection and Refinement Statistics

	Cest-2923	Cest-2923-PA	Cest-2923-IPA
PDB accession code	**4BZW**	**4C01**	**4BZZ**
Data collection			
Beamline	ID29 (ESRF)	ID23-1 (ESRF)	ID23-1 (ESRF)
Wavelength (Å)	0.9400	0.9687	0.9687
Space group	$P6_322$	$C2$	$P622$
Unit-cell parameters (Å)	$a = b = 141.65$, $c = 165.74$ $\alpha = \beta = 90^o$, $\gamma = 120^o$	$a = 244.9$, $b = 141.4$, $c = 82.69$ $\alpha = \gamma = 90^o$, $\beta = 90.0^o$	$a = b = 141.72$, $c = 82.29$ $\alpha = \beta = 90^o$, $\gamma = 120^o$
Resolution range (Å)	46.37-2.15	49.20-2.30	48.97-2.99
No. of measured reflections	1,051,757	509,575	74,713
No. of unique reflections[a]	53,876 [5,215]	124,688 [12,482]	9,994 [1,306]
Mean I/σ(I)[a]	17.2 [6.2]	143.2 [46.5]	13.7 [4.1]
Completeness (%)[a]	99.9 [98.8]	99.9 [100]	99.6 [98.9]
Redundancy[a]	19.5 [18.0]	4.1 [4.3]	7.5 [7.3]
R_{merge} (%)[a]; R_{pim} (%)[a]	13.3 [51.4]; 3.1 [12.4]	14.3 [66.1]; 13.6 [60.9]	11.9 [47.1]; 4.6 [18.5]
Wilson B factor (Å^2)	21.2	21.2	41.98
Molecules/non-H atoms			
Protein	2/4,332	6/12,897	1/2,144
Water	503/503	1,014/1,014	4/4
Sulphate	9/45	8/40	4/20
Acetate	3/12	6/24	3/12
Other molecules	1/8	17/86	1/3
Refinement			
R_{work}(%)/R_{free}(%)	15.5/19.5	22.5/27.9	15.6/21.4
Average B-factors (Å^2); protein	27.0	41.0	49.7
Average B-factors (Å^2); water	39.1	38.7	45.2
Average B-factors (Å^2); other	76.0	64.8	94.2
rms deviation bond length (Å)	0.007	0.008	0.008
rms deviation Angles (°)	1.000	1.160	1.060
Molprobity			
Ramachandran favoured (%)	97.0	92.0	95.0
Ramachandran outliers (%)	0.0	0.3	0.0

[a]Values for the highest resolution shell are given in brackets.

Table 2. Kinetic parameters for pNPA and pNPB hydrolysis by Cest-2923.

Substrate	V_{max} (μmol min^{-1} mg^{-1})	K_m (mM)	k_{cat} (s^{-1})	k_{cat}/ V_{max} (s^{-1} mM^{-1})
pNPA	660 ± 50	1.7 ± 0.2	343.6 ± 26	202 ± 28
pNPB	40 ± 8	7.6 ± 1.2	20.8 ± 4	2.7 ± 0.7

Enzyme activities were determined at 30 ºC in 50 mM sodium phosphate buffer, pH 7.0. Results are the mean value ± SD from three independent experiments.

Three dimensional superposition of Cest-2923 from this work with models deposited by structural genomics consortia (3d3n from NSGC; 3bxp from JCSG).

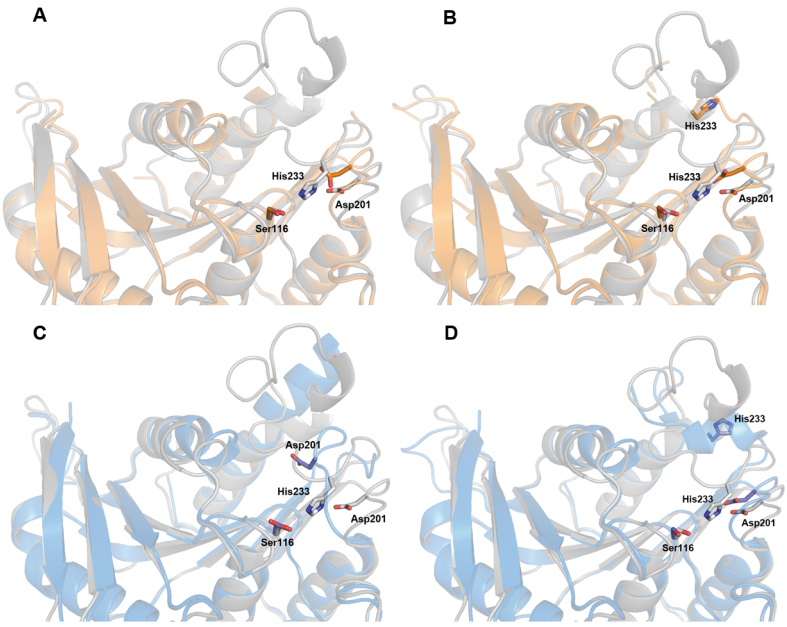

Fig. S1. Three dimensional superposition of the Cest-2923 model (chain A) from this work (shown as *grey cartoon*; PDB entry: 4bzw) with: (A) chain A, (B) chain B of PDB entry 3d3n deposited by the Northeast Structural Genomics Consortium (shown as *orange cartoon*), and (C) chain A, (D) chain B of PDB entry 3bxp deposited by the Joint Center for Structural Genomics (shown as *blue cartoon*). In all models, amino acid residues of each model from the catalytic triad are shown as *sticks* with the same colour code as the *cartoon* models.

Figure S2. Far-UV CD analysis of Cest-2923 at neutral and acidic conditions.

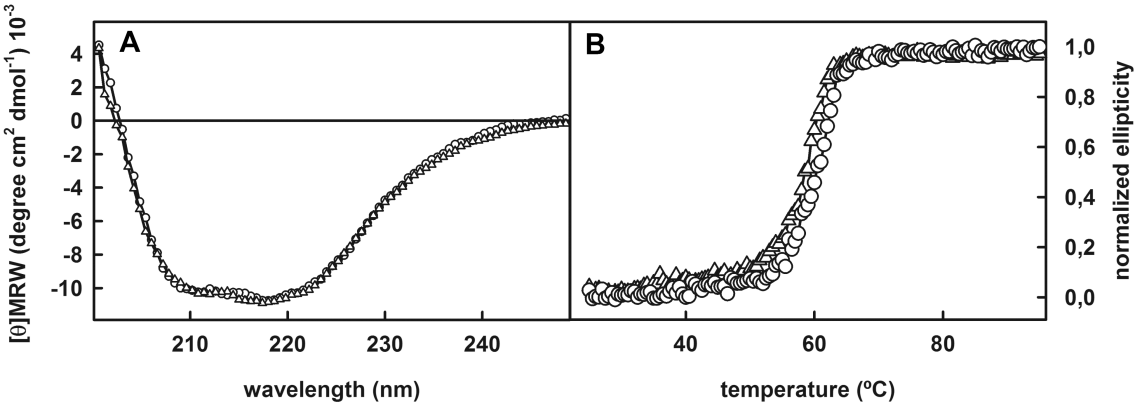

Fig. S2. (A) Far-UV CD spectra of Cest-2923 from *Lactobacillus plantarum* WCFS1 at neutral (20 mM Tris-HCl, pH 8.0 with 0:1 M NaCl) (open circles) and acidic (20 mM sodium acetate, pH 5.5 with 0.1 M NaCl) (open triangles) conditions. Protein concentration was 6.5 μM (0.2 mg/ml). (B) Heat denaturation curves for Cest-2923 in the same experimental conditions as in panel A (see Materials and Methods).

Figure S3. Analytical ultracentrifugation studies of Cest-2923 at basic conditions indicate a predominance of tetramers over dimers, similarly to acidic conditions.

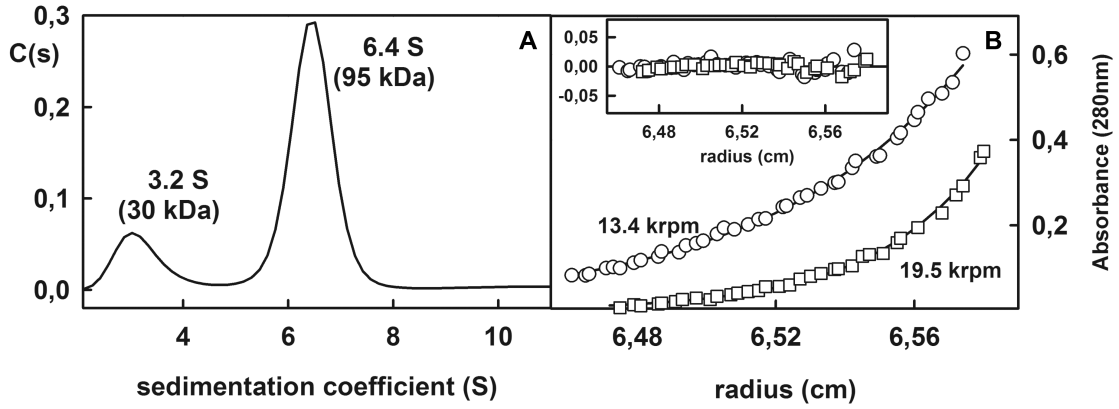

Fig. S3. Analytical ultracentrifugation analysis of Cest-2923 at basic conditions. (A) Sedimentation coefficient *c(s)* distributions for Cest-2923 (13 μM) in Tris buffer (20 Tris-HCl, pH 9.0 with 0.1 M NaCl). Raw sedimentation velocity profiles for this analisys were acquired using absorbance at 280 nm, 45,000 rpm, 20 ºC, and different times (not shown). Calculations were done with the program SEDFIT [33]. (B) Sedimentation equilibrium analysis of Cest-2923 (13 μM) in Tris buffer (20 mM Tris-HCl, pH 9.0 with 0.1 M NaCl) at 13,400 rpm (*open circles*) and 19,500 rpm (*open squares*). Absorbance at 280 nm is plotted against the radial position from the centre of the rotor. The fit to the data set (*solid line curves*) corresponds to a monomer-tetramer association equilibrium. Residuals from this fit are shown in the inset.

Figure S4. Three dimensional comparison of non-canonical tetramers of Cest-2923 and canonical tetramers of enzymes from the HSL family.

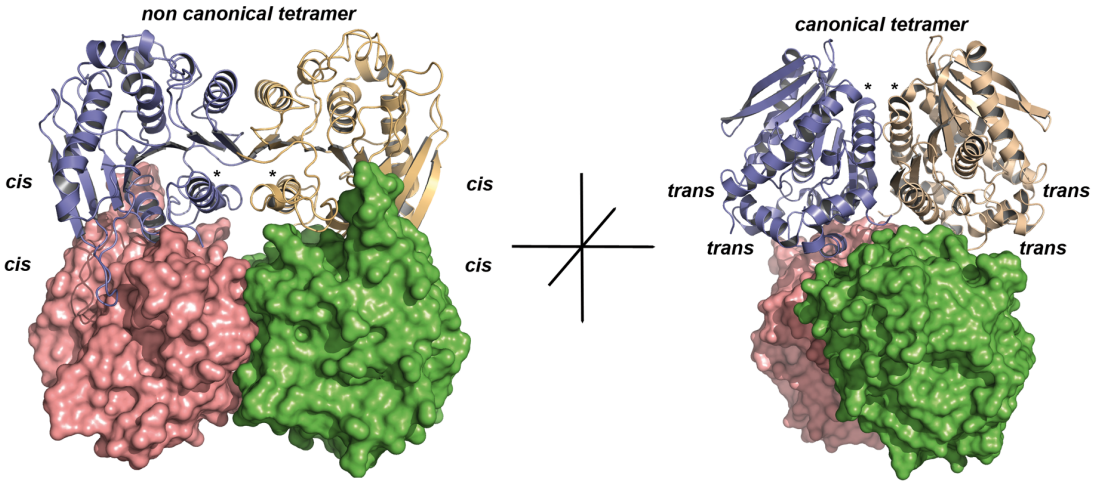

Fig. S4. Comparison between non-canonical and canonical tetramers. *Left*, non-canonical tetramer of Cest-2923. Subunits of one dimer are shown as *cartoon* models in *blue* and *wheat* colours, and the others from the accompanying dimer are shown as *surface* (*salmon* and *green*). Asterisks indicate the approximate position of the C-terminal α-helix, which defines the *cis* face of the subunits (see the text). *Right*, canonical tetramer of the hyperthermophilic esterase EstE1 (PDB entry: 2c7b) [15]. The colour code is the same as in the non-canonical tetramer of Cest-2923. The reference lines indicate the two-fold symmetry axes characteristic of both assemblies, i.e., they exhibit a 222 point group symmetry.

Figure S5. The presence of acetate molecules in the close vicinity of the nucleophile Ser116 in Cest-2923 crystals soaked with substrates reveal catalysis within the crystal.

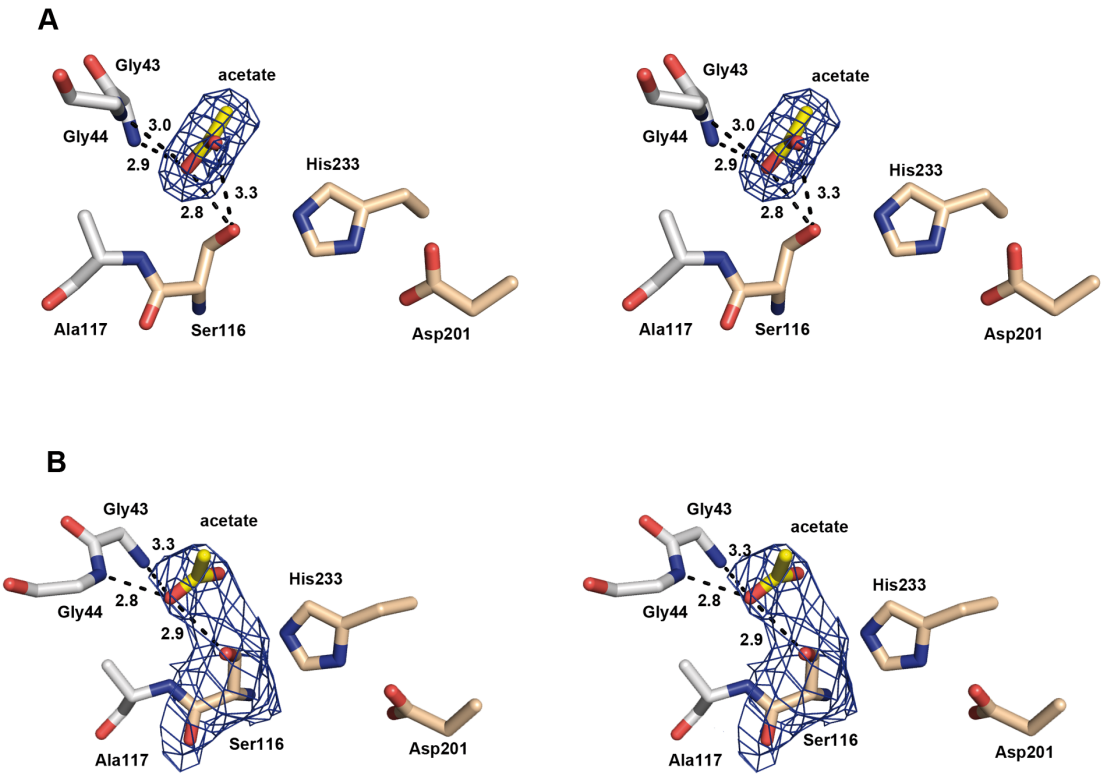

Fig. S5. Acetate molecule close to the nucleophile Ser116 in crystals soaked with the substrates phenyl acetate (PDB entry: 4c01) (A) or isopropenyl acetate (PDB entry: 4bzz) (B). Stereo views have been prepared in both cases. Hydrogen bonds involving the acetate molecule are shown as *black, broken lines*. Residues of the catalytic triad are shown as *sticks* in *wheat* colour. Other residues are shown as *grey*, *sticks*. The composite map calculated with *SFCHECK* (*2Fo - Fc* in *blue*; contoured at 1-σ level) is shown around the acetate molecule and the nucleophile. Distances are given in Å.